2013-07-12

The Effect of Cooling Rate of Friction Stir Welded High Strength Low Alloy Steel

Scott Anthony Rose
Brigham Young University - Provo

The Effect of Cooling Rate on Friction Stir Welded High Strength Low Alloy Steel

Scott Rose

A thesis submitted to the faculty of
Brigham Young University
in partial fulfillment of the requirements for the degree of

Master of Science

Tracy W. Nelson, Chair
Carl D. Sorenson
Michael P. Miles

Department of Mechanical Engineering

Brigham Young University

June 2013

ABSTRACT

The Effect of Cooling Rate on Friction Stir
Welded High Strength Low Alloy Steel

Scott Rose
Department of Mechanical Engineering, BYU
Master of Science

The friction stir welding of steel has produced a hard zone in several different alloys. Despite its detrimental effects on weld toughness, the reasons behind neither its formation nor a method of reducing its size or effects have been explored. Recent advances in process control allow for direct heat input control, which combined with the use of backing plates of different thermal conductivity allows for an expansion of the process window. These control methods also affect the HAZ cooling rate by providing greater range (a 60% increase compared to a fixed backing plate) and control (five welds within 16 °C/s). This increased range produced microstructures consisting of various forms of ferrite at lower cooling rates and bainite at higher cooling rates. The hard zone was determined to be the result of the formation of the bainite at higher cooling rates and was avoided by keeping the cooling rate below 20 °C/s in HSLA-65.

Keywords: cooling rate, microhardness, microstructure, FSW, HSLA-65,

ACKNOWLEDGMENTS

I would like to thank my committee for their advice and direction on my research. I would also like to thank my family for their encouragement and support throughout grad school. Most especially, I am indebted to my wife who pushed me and helped me get through all the bumps that came along the way.

Funding for this work was provided by the National Science Foundation's Industry/University Cooperative Research Center Program and the Center for Friction Stir Processing under grant number IIP-0934377.

TABLE OF CONTENTS

LIST OF TABLES

LIST OF FIGURES

1 INTRODUCTION

Steel has a large variety of structural and other applications due to its vast range of properties. High-strength low-alloy steels are a sub-class of steel which have high strength and toughness because of their carefully controlled and refined microstructure.

Due to the size and complexity of many products, joining is a necessary manufacturing step for steel. Arc welding is the most common form of joining used in steel fabrication.

Arc welding is a fusion process where the base metal is melted with an electric arc and the subsequent solidification of the weld pool produces the joint. This process involves very high peak temperatures and often results in the reduction of the mechanical properties such as strength and toughness.

Friction stir welding is a hot deformation joining process which occurs at much lower temperatures than arc welding. These lower temperatures aid in preventing the property degradation that occurs in arc welding. In addition to being oftentimes stronger and tougher than their arc welded counterparts, friction stir welds in steel have strength and toughness that are comparable to, or better than, the base metal.

An area of concern in friction stir welded steels is the region of high hardness that is often observed in the advancing side of the weld nugget. This hard zone has been shown to decrease weld toughness.

To date, studies have only observed the hard zone and not explored the reasons behind its formation, nor the methods of reducing its effects. This study aims to understand how changes in the friction stir weld process parameters affect the hard zone in HSLA-65 steel.

2 LITERATURE REVIEW

2.1 High-Strength Low-Alloy Steels

High-strength low-alloy (HSLA) steels are a branch of low carbon steels whose high strength comes from grain refinement of the material microstructure. In addition to their high strength, these steels also have improved weldability, formability, and toughness [1, 2]. The fine grain size of HSLA steels are a result of microalloying and thermo-mechanical control processes (TMCP).

Microalloying is the use of small amounts of alloying elements (primarily Molybdenum, Vanadium, Niobium, and Titanium) to form carbides that inhibit grain growth [1, 3]. The ASTM A945 chemical requirements for grade 65 HSLA steel are listed in Table 2-1 [4].

Table 2-1 – Chemical requirements of HSLA-65 steel. Source : [4]

C	Mn	P	S	Si	Ni	Cr	Mo	Cu	V	Nb	Al	Ti	N
0.10	1.10-1.65	0.03	0.01	0.10-0.40	0.40	0.20	0.08	0.35	0.10	0.05	0.08	0.007-0.020	0.012

All values maximum unless a range is listed

TMCP is a combination of deformation and thermal processes which change the microstructure during production. These processes affect the strain, strain rate, temperature and cooling rate of the material. These effects change the grain size and the morphology of the material [5]. The resultant microstructure determines the mechanical properties of the material.

Despite the degree of control that can be had on the microstructure during production, the size and complexity of most modern structures requires joining. This often leads to welding. Welding introduces an additional thermal cycle to the as-received material which alters the carefully constructed microstructure developed through TMCP.

2.2 **Arc Welding**

Arc welding is the most commonly used welding process in industry, but it can have several deleterious effects on the material microstructure. The weld nugget is a region of cast microstructure that is formed upon solidification of the molten weld pool. The heat-affected zone (HAZ) is formed when the high temperatures of the molten pool conduct to the surrounding material.

These high temperatures cause a large amount of grain growth, often leading to the development of a coarse-grained heat affected zone (CGHAZ). The HAZ also experiences high cooling rates resulting in morphologies such as bainite and martensite. These microstructures tend to be very hard and brittle [6, 7].

For HSLA-65, Sampath emphasized that secondary processing methods, like welding, need to try to "retain or recreate microstructures" [1]. This is done in an effort to maintain the carefully constructed properties of HSLA steels. Process control in arc welding focuses on control of the cooling rate and heat input.

Cooling rate control is achieved through varying the preheating condition and the weld heat input. Cooling rate is inversely proportional to changes to these parameters [8, 9].

Heat input control is primarily accomplished by changing the weld power (P) and travel speed (v). The relationship between heat input (HI) and these variables is [8]:

$$HI = P/v \quad \textbf{(2-1)}$$

Weld power is the product of the arc voltage and current [8], and is proportional to the weld temperature according to the principles of thermal circuitry [10].

Because the peak temperature is always greater than or equal to the melting temperature, it is difficult to eliminate the cast microstructure of arc welds. Thus control of the heat input and cooling rates is primarily aimed at reducing the deleterious effects to the microstructure through HAZ width reduction and avoidance of adverse phase changes that occurs in the CGHAZ.

2.3 **Friction Stir Welding**

Friction stir welding (FSW) is an elevated temperature deformation process that has successfully been used to join metals. This process produces microstructures that retain a fine-grained, wrought microstructure, much closer to that of the as-received plate [11, 12].

The peak temperatures in FSW of steels are estimated to be in the range of around 1000 to 1200 °C, or about 70 to 80% of the melting temperature [11-14]. These lower temperatures, while sufficient to prevent the formation of the CGHAZ common in arc welding, still produce an HAZ [11].

FSW is also beneficial to the mechanical properties of steel. Steel friction stir welds have been shown to have tensile strength comparable to, or stronger than, the base metal [11, 12]. The toughness has also been shown to be higher than the base metal by several investigators [15-17].

Despite the increase in overall toughness, a hard zone has been observed on the advancing side of the weld nugget [13, 18, 19]. The hard zone is an inhomogeneous region of higher than average hardness. This is a concern because these inhomogeneities have been observed to decrease weld toughness [17, 20]. Examples of the hard zone are observed in Figure 2-1 in the advancing side of the weld nugget in both welds of higher heat input.

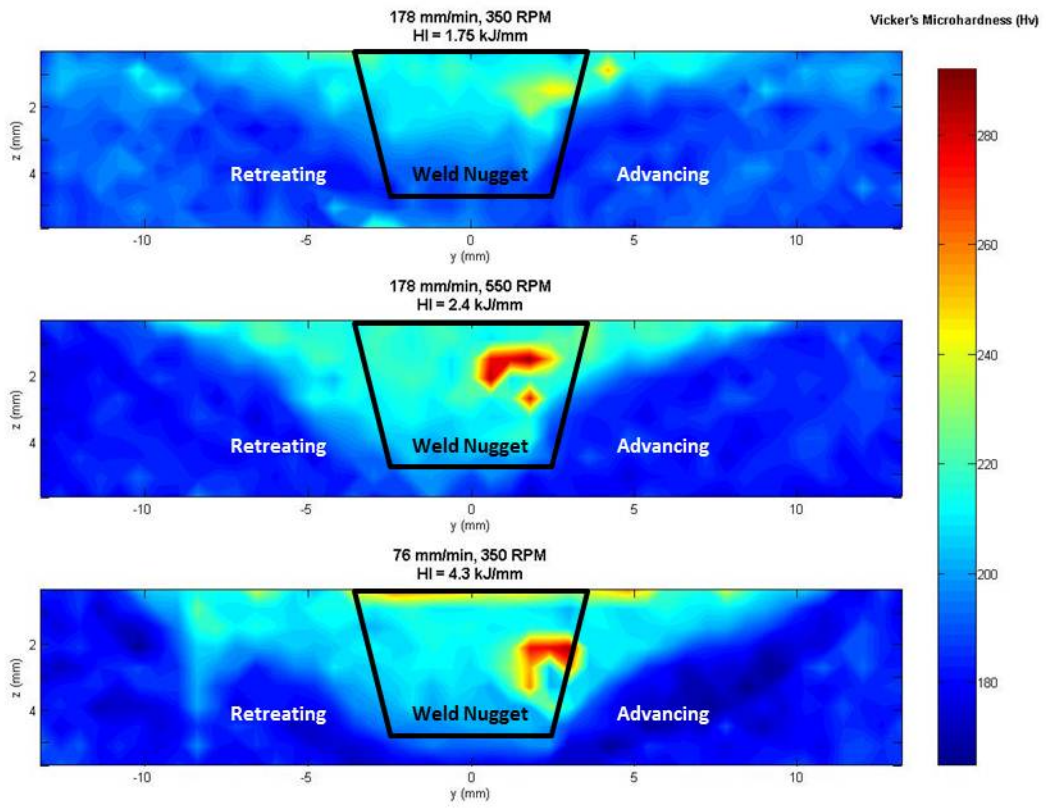

Figure 2-1 – Hardness maps (HV) of FSW of X-65. Source: [19]

This hard zone has been observed across several different alloys and welding parameters [13, 18, 19]. Table 2-2 highlights some of the alloys, hardness values, and welding parameters where the hard zone has occurred. The hard zone region was observed to be 10 to 40% higher than rest of weld with the difference in hardness value increasing with increased alloy strength.

Table 2-2 – Hard zone characteristics and parameters. Sources: [13, 18, 19]

Steel Alloy	Average Weld Hardness (HV)	Peak Hardness (HV)	Difference (HV)	Rotational Speed (RPM)	Travel Speed (IPM [mm/min])
1018	160	175	15	450-650	1-4 (25-100)
X65	220	280	60	350, 550	3, 7 (75,175)
X80	250	350	100	550	4 (100)
L80	400	500	100	450, 550	4, 4 (100,100)

Some have proposed that the hard zone is a result of high peak temperatures or high heat inputs. Ozekcin et al. suggested that the high hardness is a result of high peak temperatures causing austenite grain coarsening [13]. Nelson et al. also observed that the hard zone occurred in welds of high peak temperature, as a result of high heat input [19]. Grain refinement, due to fast cooling rates, has also been suggested to be a cause of the hard zone [13]

Some studies have used physical weld simulations, such as hot compression and hot torsion tests, to observe the effects that strain, strain rate, peak temperature, and cooling rate have on the weld microstructure. Matsushita et al. varied the peak temperature, strain, and strain rate while holding the cooling rate constant in hot compression samples [21]. They found that the strain and strain rate had a negligible effect on the microstructure while the thermal effects had a much larger influence on the microstructure [21]. Allred varied peak temperature, strain rate, and cooling rate in hot torsion tests and found that the microstructure was significantly affected by the peak temperature and cooling rate [22].

The findings of Matsushita and Allred suggest that in order to control the microstructure in FSW, control over the peak temperature and cooling rate are needed. To date, no studies have controlled the cooling rate and peak temperature during FSW.

FSW process control has typically been performed through variations to the rotational and travel speeds. Several relationships have been developed to correlate these speeds to the weld outputs. These relationships are the pseudo heat index (PHI) [23], advance per revolution (APR) [11], and heat input [24]. Of these relationships, Wei found that the heat input had the best correlation to the weld microstructure [25].

In friction stir welding, heat input follows the arc welding relationship of equation (2-1) [24]. By varying only the rotational and travel speeds, the weld torque, and subsequently the weld power, is a dependent variable that fluctuates over the course of the weld [26, 27]. Recent advances in process control have allowed for weld power control in FSW [27]. This allows for direct heat input control by maintaining a constant power over the length of the weld.

Advances have also been made towards cooling rate control. While travel speed has a known effect on weld cooling rate [11, 14], very little has been done to exploit the weld anvil used in FSW to affect the heat flux exiting the workpiece.

Upadhay and Reynolds studied changes to the heat flux out of the workpiece through the use of the backing plate materials of different thermal conductivities [28]. Backing plate thermal conductivity was found to affect the peak tool temperature. They also observed that using backing plates of lower conductivity improved the weld homogeneity [28]. Therefore, using backing plate materials of different thermal conductivities should allow for greater control over the FSW process.

The additional process control granted by these new methods should allow for greater control over the microstructure and mechanical properties of friction stir welds. This study will show the effects that varying the parameters of these control methods have on the hard zone of HSLA-65 steel friction stir welds.

3 EXPERIMENTAL APPROACH

3.1 Weld Setup

All welds in this study were bead on plate welds performed on a MTI model RM2 FSW machine using a polycrystalline cubic boron nitride (PCBN), convex scrolled should step spiral (CS4) tool (model E44111, the tool drawing can be found in Appendix A). Welds were run in separate 6.35 mm (0.25 in) thick HSLA-65 plates. Each plate was ground on both sides to remove the mill scale. Each weld was 750 mm (29.5 in) in length.

Tool temperature data was obtained from a K-type thermocouple inserted into the tool collar. Plate temperatures were was obtained from K-type thermocouples placed in the weld plate at a depth of 3.8 mm (0.15 in) from the surface of the plate. The thermocouples were positioned in the HAZ at three different distances from the weld center and their linear positions were randomized. The exact locations can be found in Table 3-1. An example of the setup is found in Figure 3-1.

Table 3-1 – Workpiece thermocouple locations

T/C Number	1	2	3	4	5	6	7	8	9
Distance from Weld Center (in)	0.30	0.18	0.24	0.18	0.24	0.30	0.24	0.18	0.30
Distance from Weld Start (in)	21.00	21.75	22.50	23.25	24.00	24.75	25.50	26.25	27.00

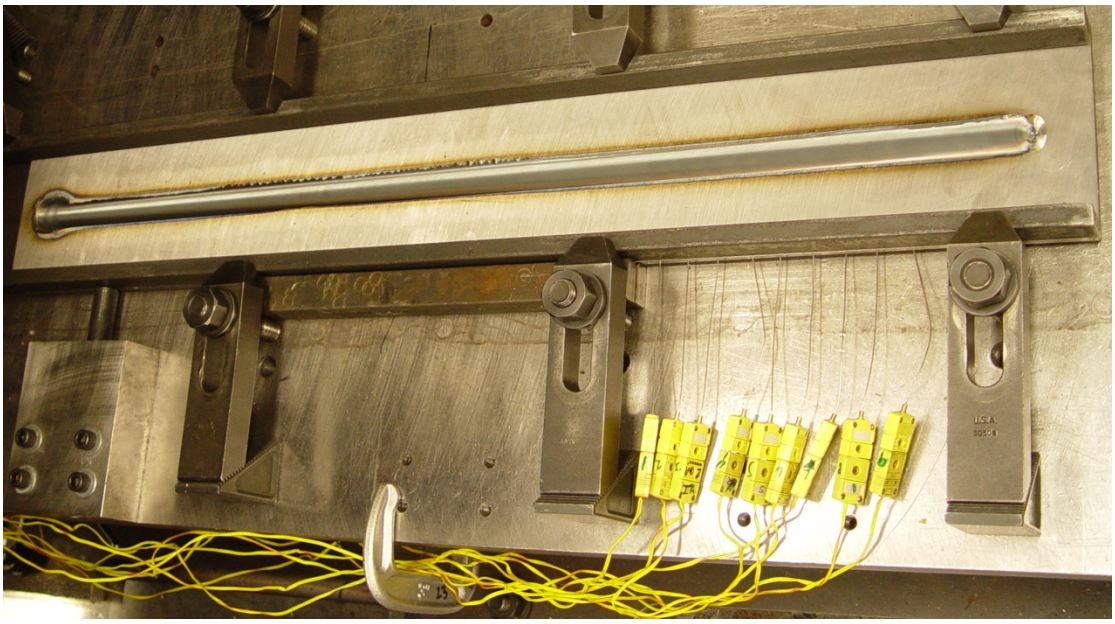

Figure 3-1 – Example Weld Setup

As the thermocouples are positioned farther from the weld center they should experience different thermal gradients. They should observe a larger thermal gradient in the horizontal direction as the temperature difference at various points inside the weld is smaller than that of the edge of the weld and the base metal. Meanwhile the thermocouples should experience a smaller thermal gradient in the vertical direction as temperature difference between the weld plate and the anvil decreases when going from the weld nugget towards the base metal.

While the exact magnitudes of the cooling rates in the different directions are not known, the weld nugget cooling rate should be higher than that measured by the thermocouples in this study but not lower.

3.2 **Design of Experiments**

A central composite face centered design (CCF) of 10 runs was developed using backing plate material and heat input as the factors [29]. The response variables used in this study were

cooling rate and 95% percentile hardness. A least squares analysis was performed for each response variable followed by an analysis of variance (ANOVA) test in JMP.

The backing plate (BP) levels were determined using the logarithm of the thermal conductivity. The heat input (HI) levels were determined using three evenly spaced power and travel speed levels, thus confounding power and travel speed with the heat input. The properties for each factor are listed in Table 3-2.

Table 3-2 – Factor levels of final design of experiments

Backing Plate Variables				Heat Input Variables			
Level	Material	k (W/m·K)	log k	Power (W)	Travel (mm/min [IPM])	Heat Input (J/mm)	Heat Input Level
-1	Granite	2.7	0.4314	3750	76 (3)	2952.76	1.5
0	AL6XN	11.8	1.0719	4500	152 (6)	1771.65	0
1	Steel	51.9	1.7152	5250	229 (9)	1377.95	-0.5

Thermal diffusivity is generally used when dealing with transient systems. Figure 3-2 compares the thermal conductivities and diffusivities of each of the backing plates used. The linear correlation between the two properties is due to the fairly constant density and specific heat of each of the backing plates. The benefit of using thermal conductivity is that it is the more commonly reported of the material thermal properties.

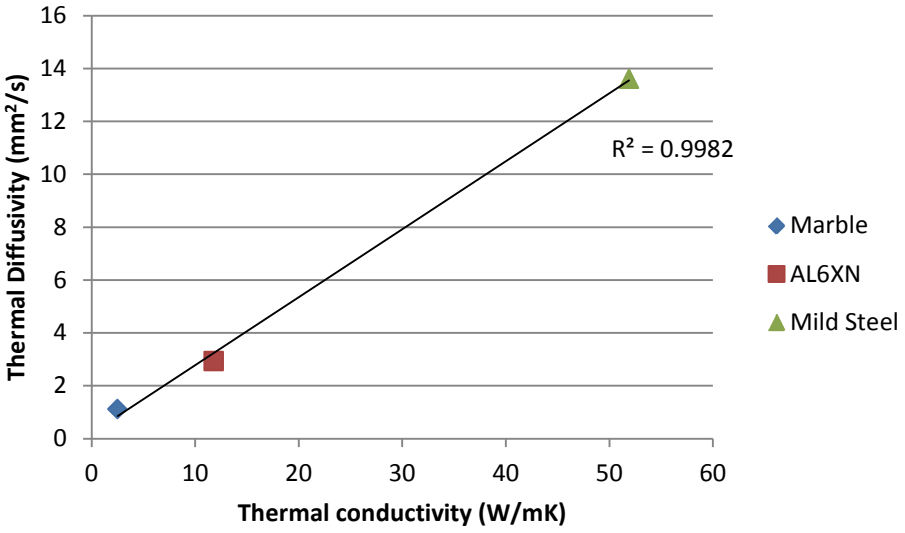

Figure 3-2 – Comparison of backing plate thermal properties

3.3 Data Analysis and Metrics

The temperatures for all of the embedded thermocouples exceeded the A_3 temperature. These temperatures were then processed in Matlab to calculate the HAZ cooling rate from 800 to 500 °C. Despite the differences in the thermal gradients in the vertical and horizontal directions, the overall magnitude of the cooling rate stayed fairly constant for each weld position. Thus, the cooling rates acquired from all the thermocouples in a weld were averaged together to give a single cooling rate per weld (Full temperature and cooling rate data can be found in Appendix C:.

Metallographic samples were taken at a location 515 mm (20.25 in) from weld start and polished to a 1 µm finish according to standard practices. Microhardness measurements were taken across each sample using a Vickers hardness indenter at 500g and a 0.3 mm grid spacing. The microhardness data was converted to a hardness map for each sample.

In order to define the hard zone of each weld, a metric to determine the weld hard zone was required. The metric that was decided upon was the 95th percentile hardness (See Appendix B for further details behind this metric). The highest density of points above this 95% hardness value was determined to be the hard zone of each weld.

Each sample was etched using a 2% Nital etch to reveal the grain boundaries for optical microscopy. Select samples were then re-polished to a 0.5 μm finish for the purpose of electron microscopy. Electron backscatter diffraction (EBSD) was performed on the hard zone of these samples in order to characterize the weld microstructure. Several lath measurements were taken across the EBSD images and were averaged together to yield a single lath width and length value for each sample.

A rough delineation also had to be made between weld metal and base metal for purposes of calculating the average weld hardness. The 50th percentile hardness all the welds was 210±4% HV. This value proved to be a good approximation of the weld outline upon examination of the weld hardness maps. Thus all values above 210 HV in each metallographic sample were included in the calculation of the average weld hardness.

4 RESULTS AND DISCUSSION

4.1 Parameter Effects on the Hard Zone

In this study, the hard zone hardness is characterized by the 95% hardness value. The 95% hardness metric was obtained by a percentile ranking of the hardness data for each weld. The N number of hardness values for each hardness map was ranked from lowest to highest hardness. The ranking excludes 0 and 100% such that the first and last points are assigned the percentile $\frac{1}{2N}$ and $1-\frac{1}{2N}$ respectively. This is done to allow for the case that the true maximum and minimum hardness of each weld are not captured during the microhardness testing. Each interior point of the ranking increased in rank at a rate of $\frac{1}{N}$ (Further details about this metric can be found in Appendix B).

Using this metric, the hardness value at the 95% point is used to represent the hard zone hardness. The 95% hardness values at each of the parameter levels used in this study are listed in Table 4-1.

Table 4-1 – Measured 95% hardness at each backing plate and heat input level

Heat Input (J/mm)	95% Hardness (HV)		
	Backing Plate Material		
	Granite	AL6XN	Steel
1378	264	280	298
1772	242	265.5*	279
2953	234	263	272

*center point hardness values are averaged

From Table 4-1, using a fixed backing plate material, variations to the heat input resulted in at least a 6% change in hardness, from 263 to 280 HV on AL6XN, to a maximum of 12% hardness change, from 234 to 264 HV on granite. At fixed heat input, increasing the thermal conductivity of the backing plate from 2.7 to 52 W/m·K increased the hardness by at least 13%, from 264 to 298 HV at the lowest heat input. This change in hardness increased with each step of heat input with a 15% increase at medium heat input and a 16 % increase at high heat input.

In order to more fully characterize the effects that variations to these parameters had on the hard zone hardness, a statistical analysis of the effect of these parameters on the hard zone hardness was performed. The results of this analysis are found in Table 4-2 and Figure 4-1.

Table 4-2 – ANOVA results (t-test) for 95% hardness

Effect: 95% Hardness (HV) R^2= 0.983791

	Intercept	BP	HI	BP*HI	BP*BP	HI*HI
Estimate	265.3571	17.8846	-28.6587	0.8462	-4.7143	16.4921
Prob.>t	<.0001	0.0003	0.0016	0.6316	0.1015	0.0061

BP: Backing Plate, HI: Heat Input

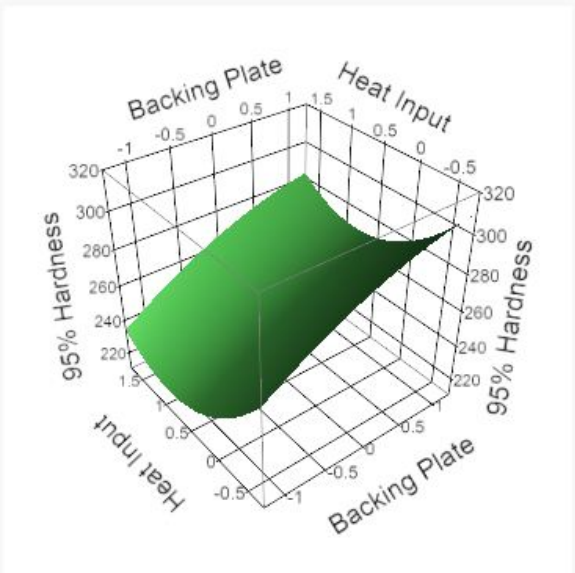

Figure 4-1 – Surface plot of the effects on 95% hardness

The heat input significantly affects the hardness. At constant backing plate thermal conductivity, the hardness increases with decreasing heat input. This increase grows at lower heat inputs as highlighted by the significance of the heat input term. The increase in hardness with decreasing heat input is contrary to the findings of Nelson et al. who observed the hard zone increase in hardness with increasing heat input [19]. Their study however, was limited to a single backing plate material.

The backing plate also has a significant effect on the hardness. At a constant heat input, the hardness increases with increasing backing plate thermal conductivity. Because heat can leave the weld faster at higher thermal conductivities, this significance cooling rate may be influencing the hardness.

4.1.1 Parameter Effects on Cooling Rate

The HAZ cooling rate for each weld at the different parameter levels used in this study is listed in Table 4-3 (Full cooling rate data for each weld can be found in Appendix C).

Table 4-3 – Measured cooling rate at each backing plate and heat input level

Heat Input (J/mm)	HAZ Cooling Rate (°C/s)		
	Backing Plate Material		
	Granite	AL6XN	Steel
1378	15.44	21.40	29.73
1772	9.26	16.78*	21.92
2953	6.97	14.52	15.62

*center point cooling rates are averaged

Changes to both the heat input and backing plate material affect the cooling rate. Using a fixed backing plate material, variations to the heat input resulted in at least 32% change in cooling rate, from 21.4 to 14.5 °C/s on AL6XN. At fixed heat input, decreasing the thermal conductivity of the backing plate decreased the cooling rate by at least a 48%, from 29.7 to 15.4 °C/s at the lowest heat input.

A statistical analysis was performed to investigate the effects of heat input and backing plate material on the cooling rate. The results of this analysis are found in Table 4-4 and Figure 4-2.

Table 4-4 – ANOVA results (t-test) for cooling rate

Effect: Cooling Rate (°C/s) R^2= 0.9884

	Intercept	BP	HI	BP*HI	BP*BP	HI*HI
Estimate	16.5729	6.5685	-9.6924	-0.7954	-0.7757	5.1524
Prob.>t	<.0001	0.0001	0.0011	0.1885	0.3205	0.0057

BP: Backing Plate, HI: Heat Input

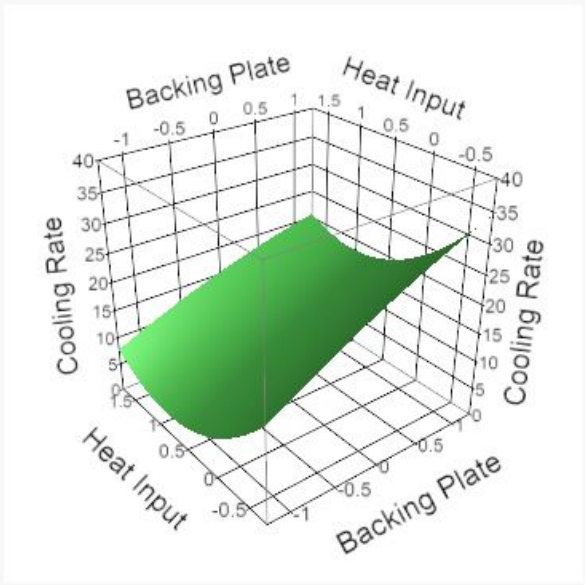

Figure 4-2 – Surface plot of the effects on cooling rate

As with the 95% hardness (Table 4-2 and Figure 4-1), the process parameters significantly affect the cooling rate and in a similar manner. How they influence the cooling rate however is better understood by known effects to the cooling rate in FSW.

In this study, travel speed is confounded with heat input, with higher travel speeds occurring at lower heat input levels (Table 3-2). Thus, the increase in cooling rate with decreasing heat input is due to the increasing travel speed at each heat input step. This correlates with the known increase in cooling rate with increasing travel speed [11, 14]. This relation between the travel speed and the cooling rate could be the reason for the significance of the quadratic heat input term.

At constant heat input, the linear change in cooling rate with backing plate is explained through the principles of conduction as a higher thermal conductivity allows for more heat to conduct away from the weld [10].

4.1.2 The Effects of Heat Input and Cooling Rate on Hardness

In arc welding, heat input and cooling rate are used to control the process in order to influence the microstructure. In order to visualize the effects of these variables in FSW, hardness maps are used to represent the microstructural changes across the weld. In Figure 4-3, the hardness maps are overlaid on a plot of the cooling rate values for each weld. The cooling rate values are grouped by backing plate material due to the large influence backing plate has on the cooling rate (Figure 4-2). Each map is identified by the acronym of each weld's backing plate material and heat input level. For example, the weld on granite with the highest heat input is labeled GH.

Comparing all of the weld hardness maps, there is a large amount of variation in the hardness characteristics across the weld parameters. Above 20 °C/s, the welds are much harder and a large hard zone is observed (AL, SM, SL). These welds also have decreased uniformity compared to welds of lower cooling rate (GH and GM). Meanwhile; welds at cooling rates less than 20 °C/s did not exhibit a discernible hard zone.

At cooling rates near 16 °C/s, there are five welds of similar cooling rate (SH, AH, AM1, AM2, GL) which, despite the differences in backing plate and heat input level, exhibit very similar hardness maps.

Figure 4-4 and Figure 4-5 compare the homogeneity of the weld microstructure, or weld uniformity. Figure 4-4 shows a weld on granite (GM) to and Figure 4-5 shows a weld on steel (SM) with both samples at the medium heat input level. This comparison is performed using optical micrographs at various locations across each weld.

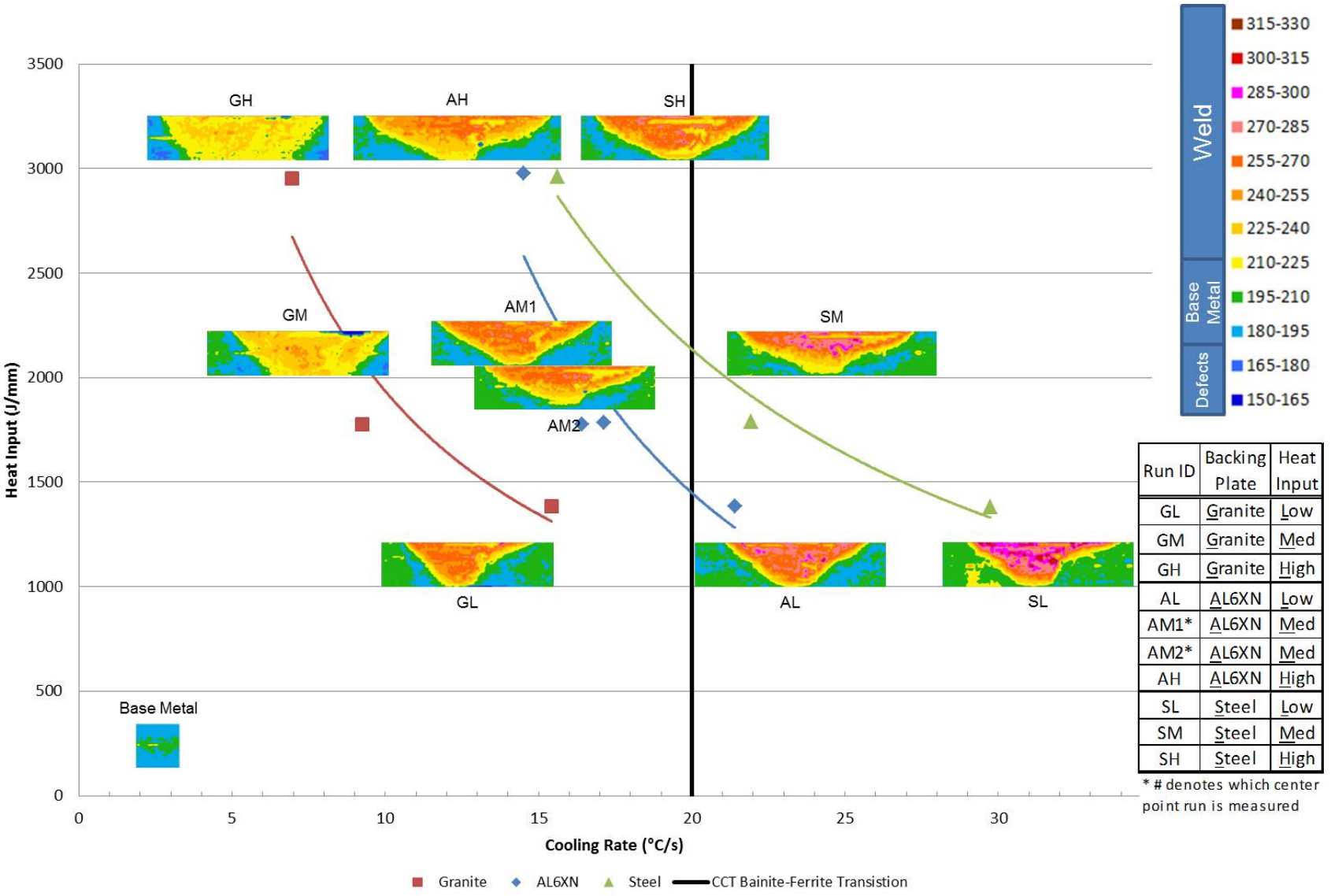

Run ID	Backing Plate	Heat Input
GL	Granite	Low
GM	Granite	Med
GH	Granite	High
AL	AL6XN	Low
AM1*	AL6XN	Med
AM2*	AL6XN	Med
AH	AL6XN	High
SL	Steel	Low
SM	Steel	Med
SH	Steel	High

* # denotes which center point run is measured

Figure 4-3 – Hardness maps (HV) of each run plotted by heat input and cooling rate.

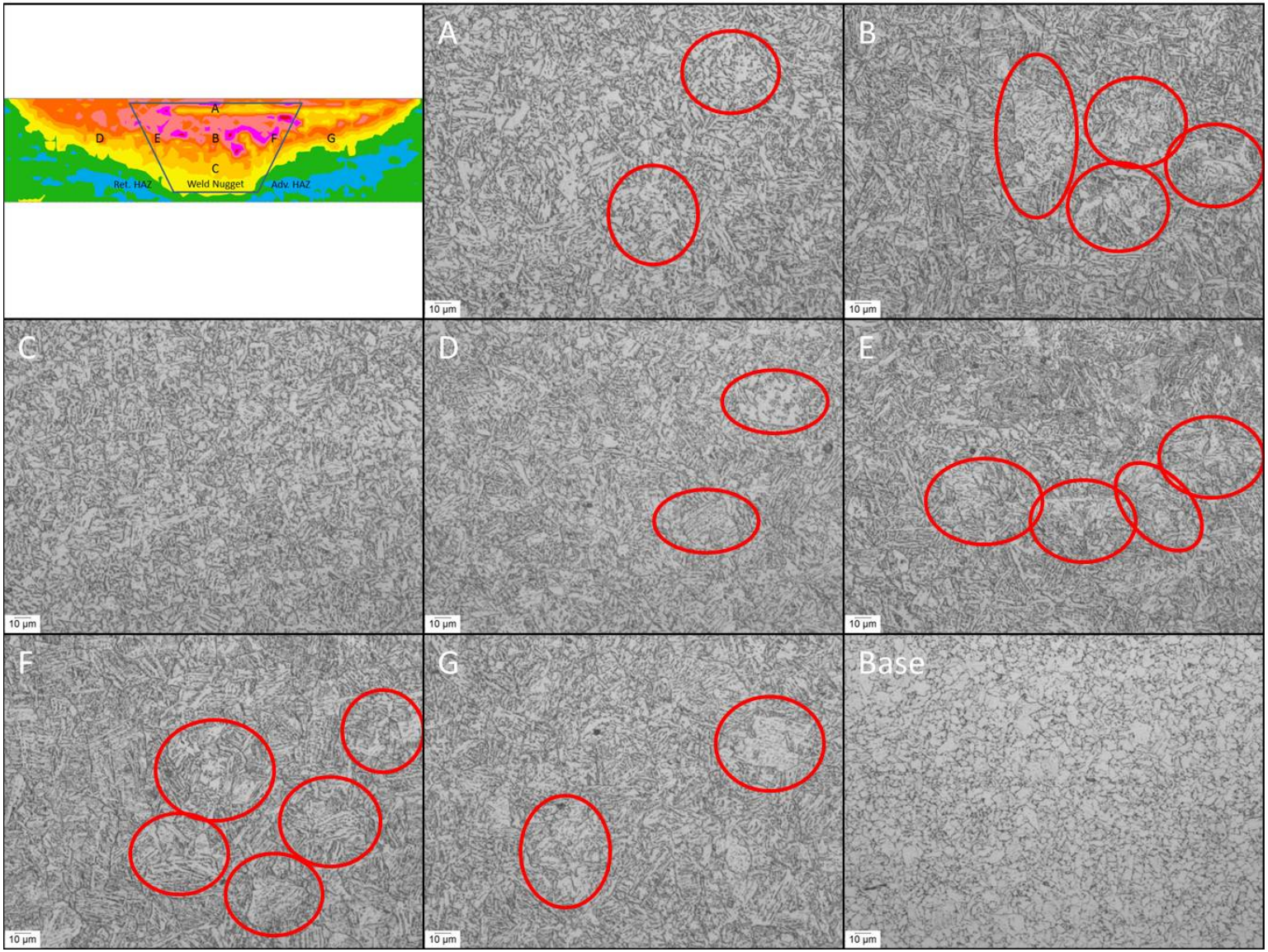

Figure 4-4 – Micrographs of medium heat input, steel backing plate weld; 500x magnification

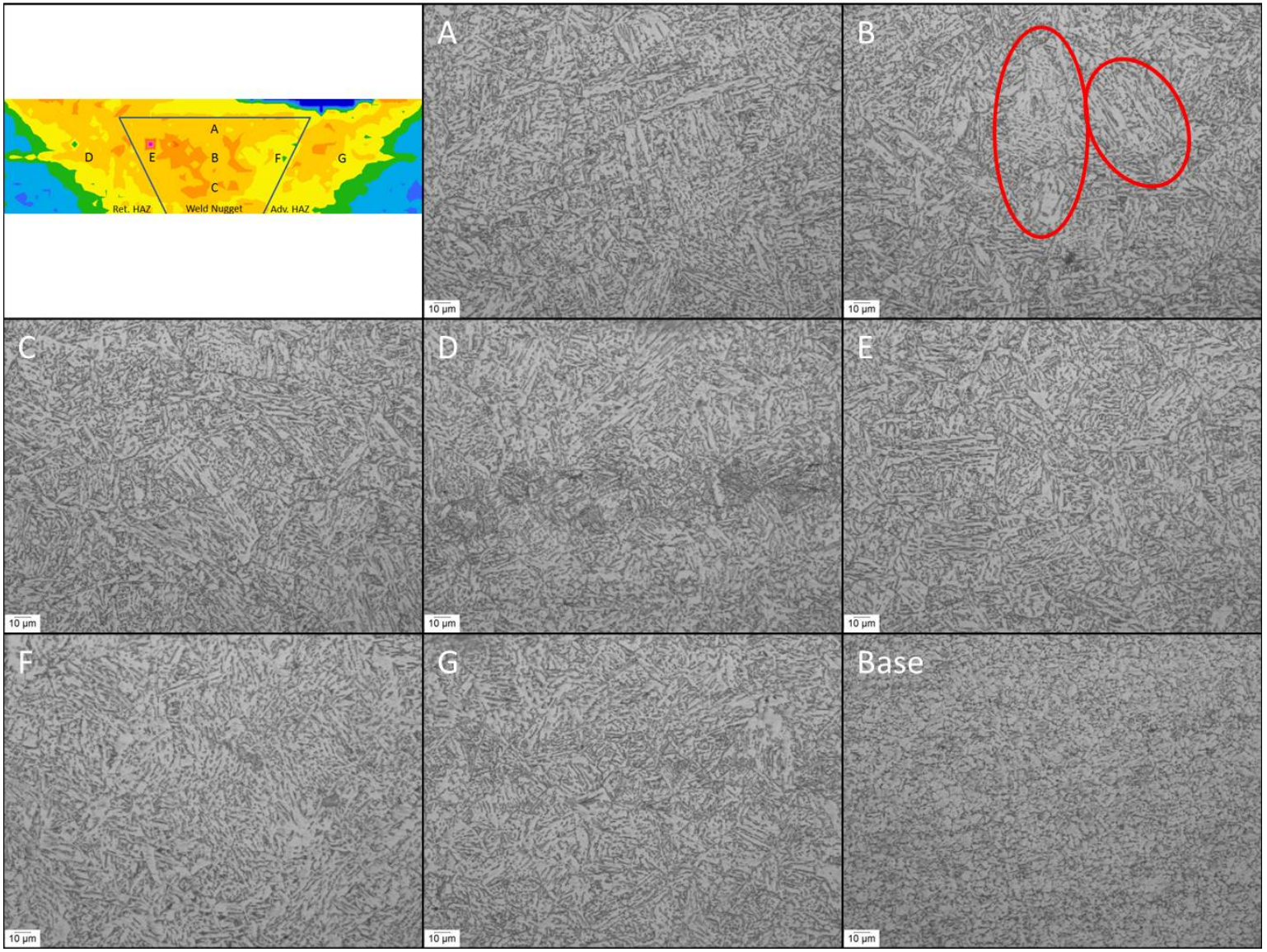

Figure 4-5 – Micrographs of medium heat input, granite backing plate weld; 500x magnification

The microstructure of the steel backing plate weld (Figure 4-4) varies in grain size both down the weld centerline (A, B, C) and across the mid-plane of the weld (D, E, B, F, G). Throughout the sample there are several regions which exhibit large grain sizes. These are marked by red ovals. These regions correspond to the areas of higher hardness in the hardness map.

The microstructure of the granite backing plate weld (Figure 4-5) remains consistent throughout the weld. The grain sizes seem to be fairly consistent throughout the sample with only occasional large grains (B).

4.1.3 Weld Hardness Relationship Quantification

The objective of this study was to understand how the process parameters affect the hard zone. In an attempt to quantify these effects, the 95% hardness was plotted against different weld process parameters. The 95% hardness values are plotted against heat input in Figure 4-6.

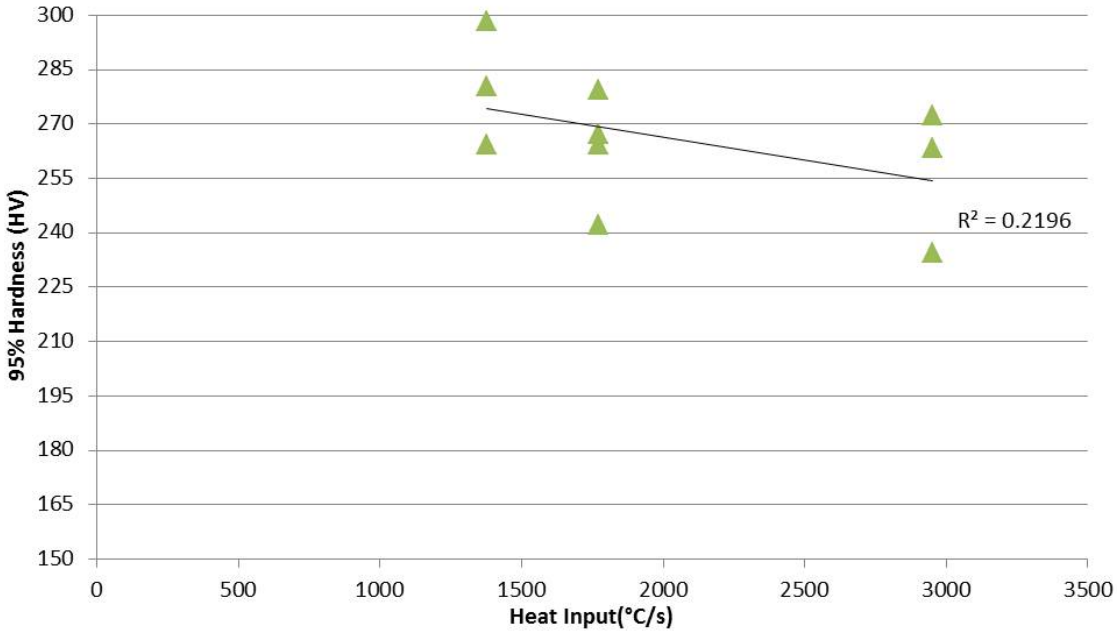

Figure 4-6 – 95% hardness by heat input

Figure 4-6 shows a poor correlation (R^2=0.2196) between the 95% hardness and heat input. Thus heat input does not capture all the changes to the 95% hardness. There is however an even distribution of the values along lines of constant heat input. This is an indication that another variable may better correlate with the 95% hardness.

These same values were grouped and fitted by backing plate material in Figure 4-7. While the individual backing plate trends fit better than heat input they still do not capture the trend for all of the data.

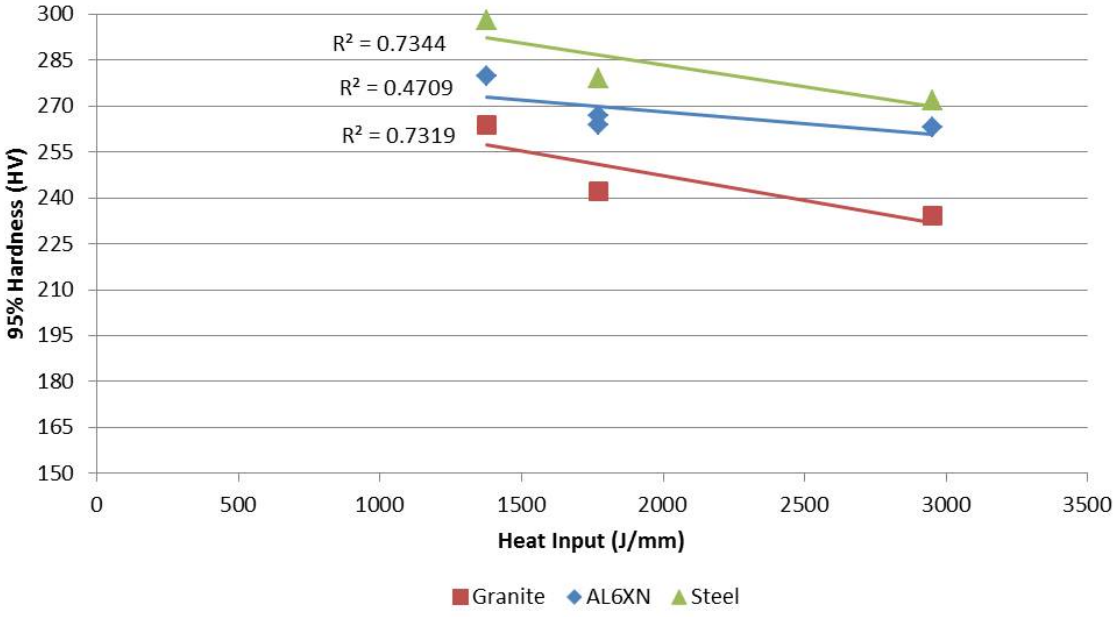

Figure 4-7 – 95% hardness by heat input, grouped by backing plate

Further analysis of the different parameter effects helped determine the parameters that best correlated with the changes to the 95% hardness. The following points suggest that the cooling rate has an effect on the 95% hardness:

- The improved fits of the backing plate curves in Figure 4-7

- The significant effect that backing plate had on cooling rate (Table 4-4 and Figure 4-2)
- The similarities between the 95% hardness and cooling rate surface plots (Figure 4-1 and Figure 4-2)

Thus the 95% hardness was plotted against the cooling rate in Figure 4-8.

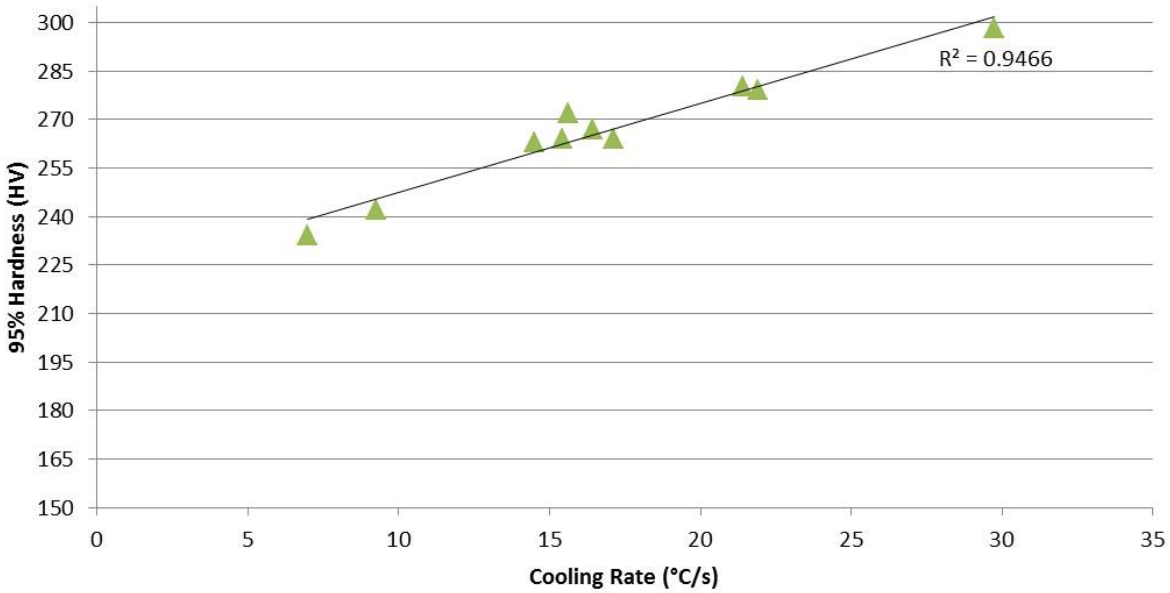

Figure 4-8 – 95% hardness by cooling rate

Unlike the trends in Figure 4-6 and Figure 4-7, Figure 4-8 shows a strong linear relationship between cooling rate and the 95% hardness. The curve fit of Figure 4-8 shows that this relationship encompasses all of the weld data (R^2=0.9466) accounting for all but 5.4% of the variation.

This relationship between hardness and cooling rate is not limited to the 95% hardness. A comparison between the cooling rate and other hardness characteristics is found in Table 4-5. Each of the measured hardness characteristics increased with increasing cooling rate.

In the literature, the hard zone was observed when the difference between the peak and average hardness exceeded 10% (Table 2-2) [13, 18, 19]. The hard zone was observed when the difference between the 95% hardness and average weld hardness was greater than 10% (Table 4-5 and Figure 4-3). In this study this occurred when the cooling rate exceeded 20 °C/s. The reason that this study observed several welds with a hardness difference of less than 10% is due to the introduction of backing plate variation.

Table 4-5 – Averaged hardness characteristics for different cooling rate ranges

Cooling Rate	Average Weld Hardness (HV)	95% Hardness (HV)	Difference (HV)	% Difference
<10 °C/s	225	238	13	6%
16 °C/s	243	266	23	9%
22 °C/s	251	280	28	11%
30 °C/s	260	298	38	14%

Only a small range of cooling rates are possible on the traditional steel backing plate. In this study, only one heat input value was capable of achieving a cooling rate less than 20 °C/s on a steel backing plate. By allowing for variation of the backing plate material, the process window was enlarged and the hard zone was avoided by achieving cooling rates less than 20 °C/s.

The difference between the 95% and average hardness can also be used to quantify weld uniformity. As the difference value decreases the weld uniformity increases. In this study, the weld uniformity increased with decreasing cooling rate. The benefit of this uniformity increase on the microstructural homogeneity was observed in Figure 4-4 and Figure 4-5. This agrees with Upadyhay and Reynolds' observations in friction stir welded aluminum [28].

As the microstructure and the hardness become more uniform, the toughness should also improve according to Tribe's findings [17]. Thus as the hard zone is eliminated with the reduction in cooling rate so too are the toughness concerns in the friction stir welding of HSLA steels due to the hard zone.

4.2 **Cooling Rate Effects on Microstructure**

In addition to affecting the hardness, cooling rate also affects the microstructure. In material science, the relationship between cooling rate and microstructure is described by continuous cooling transformation (CCT) diagrams.

CCTs are used to predict microstructure as a function of cooling rate [30]. A CCT of X-65, an ASTM A945 compliant HSLA alloy, is found in Figure 4-9 [2, 31, 32]. As the alloy cools at rates faster than 20 °C/s, the microstructure should transform into bainite. Material cooling at slower rates should form polygonal and allotriomorphic ferrite before forming a finer lath microstructure.

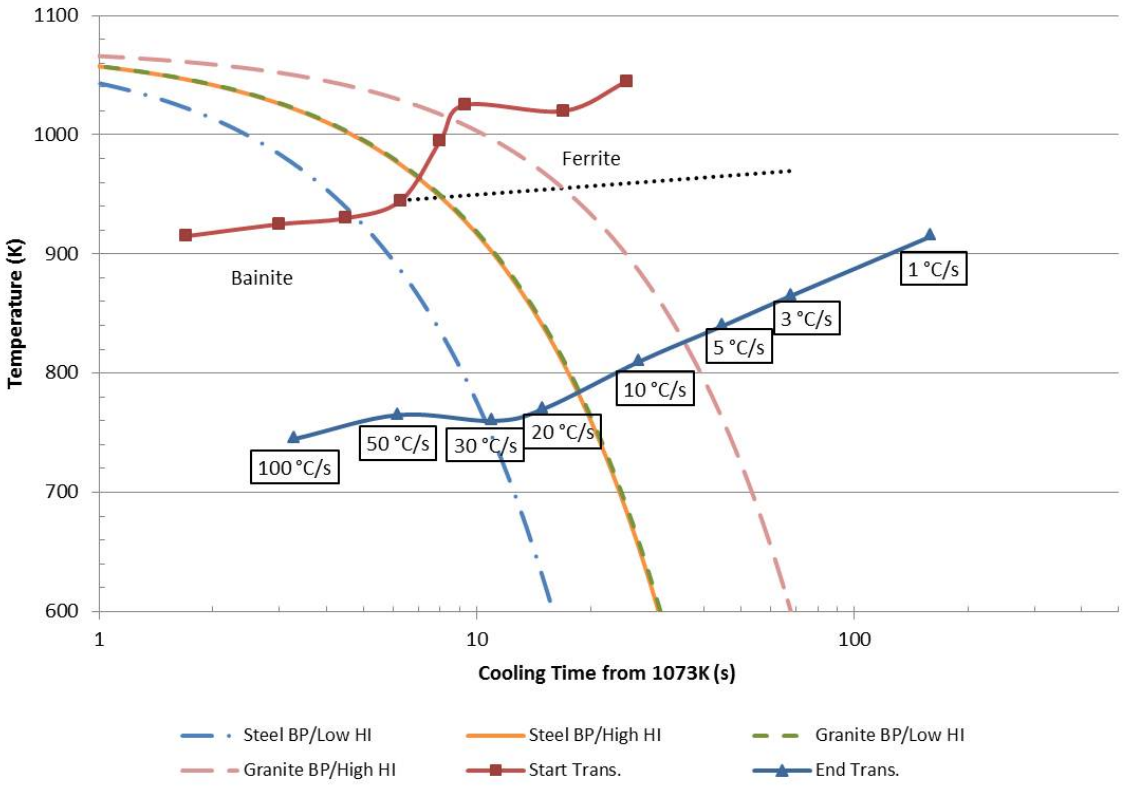

Figure 4-9 – CCT diagram for X-65 with four HAZ cooling rates. Source: [32]

The cooling rates displayed in Figure 4-9 represent the measured HAZ cooling rates of four welds (SH, SL, GH, and GL, Figure 4-3). While the cooling rates at the weld center may be slightly higher than what was measured in this study, they will not be lower. (Full temperature and cooling rate data for each weld can be found in Appendix C). Figure 4-10 shows the hard zone microstructures for these welds.

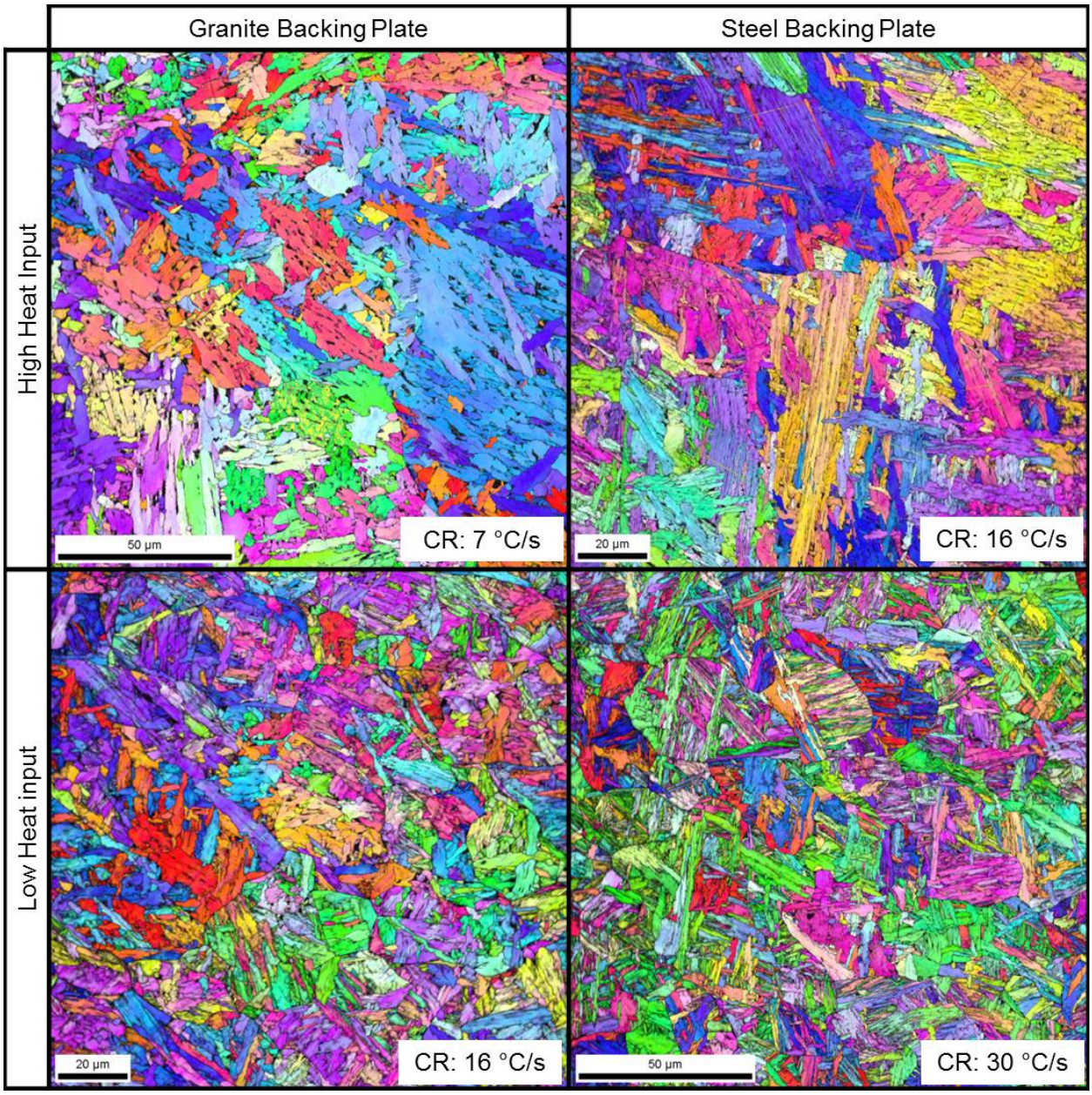

Figure 4-10 – EBSD images of four weld hard zones.

The low cooling rate weld (~7 °C/s) developed polygonal and allotriomorphic ferrite as well as developing a coarse lath microstructure. Near 16 °C/s, the polygonal and allotriomorphic ferrite was smaller than the low cooling rate weld and the lath structure that developed was much finer. The predominant microstructure in both samples is the lath structure. The high cooling

rate weld (~30 °C/s) developed bainite upon austenite decomposition with finer laths than all the other welds. These observed microstructures correspond with Figure 4-9.

The formation of bainite at cooling rates faster than 20 °C/s correlates with the observations of the hard zone above this critical cooling rate (Figure 4-3). Thus, the hard zone is primarily the result of the formation of bainite at faster cooling rates. Further analysis was performed on the microstructure data to confirm this relationship.

4.2.1 Parameter Effects on Lath Structure

From Figure 4-10, it appears that both heat input and backing plate material have an effect on the characteristics of the lath structures. Both welds of high heat input have much longer laths than the low heat input welds.

In order to quantify this length, point measurements were taken for the longest lath of five packets in each sample (Lath length images and measurements can be found in Appendix E:). These points were then used to calculate a lath's length which was then averaged together to yield a single length per sample. These average lath lengths are plotted against the heat input in Figure 4-11.

The lath length increased with increasing heat input regardless of the backing plate material. Increasing the heat input by 1575 J/mm increased the length of the laths by at least 12 μm. As laths typically do not cross the austenite grain boundaries [30], these lengths roughly correlate with the prior austenite grain size. Thus with increasing heat input, the prior austenite grain size increases. This is in agreement with previous observations [13, 19, 25].

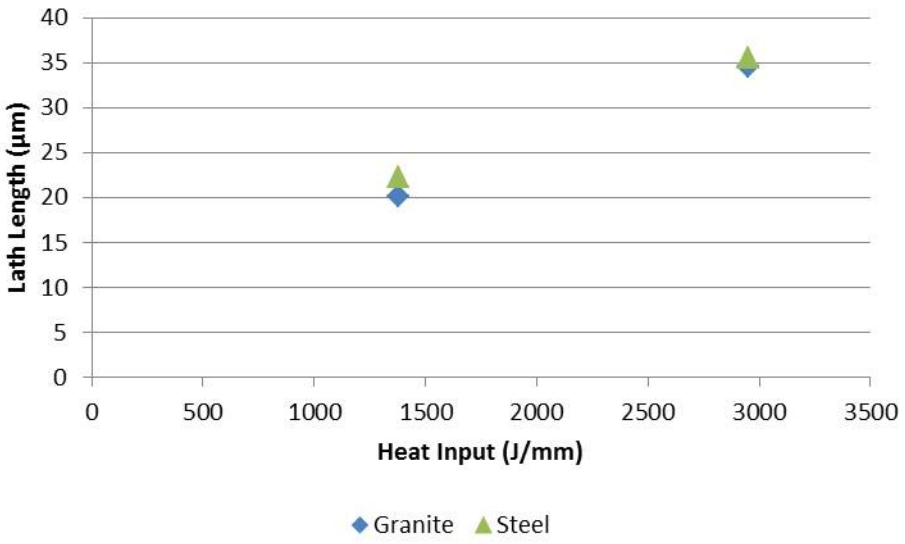

Figure 4-11 – Average lath length by heat input

The lath width also appears to be finer for the welds made on a steel backing plate (Figure 4-10). The lath widths were obtained using the same method as Wei [25]. The measured lath widths are listed in Table 4-6 for each sample. A visualization and surface fit of the measurements are found in Figure 4-12

Table 4-6 – Average lath width by backing plate and heat input level

	Lath Width (µm)	
Heat Input (J/mm)	Backing Plate	
	Granite	Steel
1378	0.88	0.59
2953	1.11	0.81

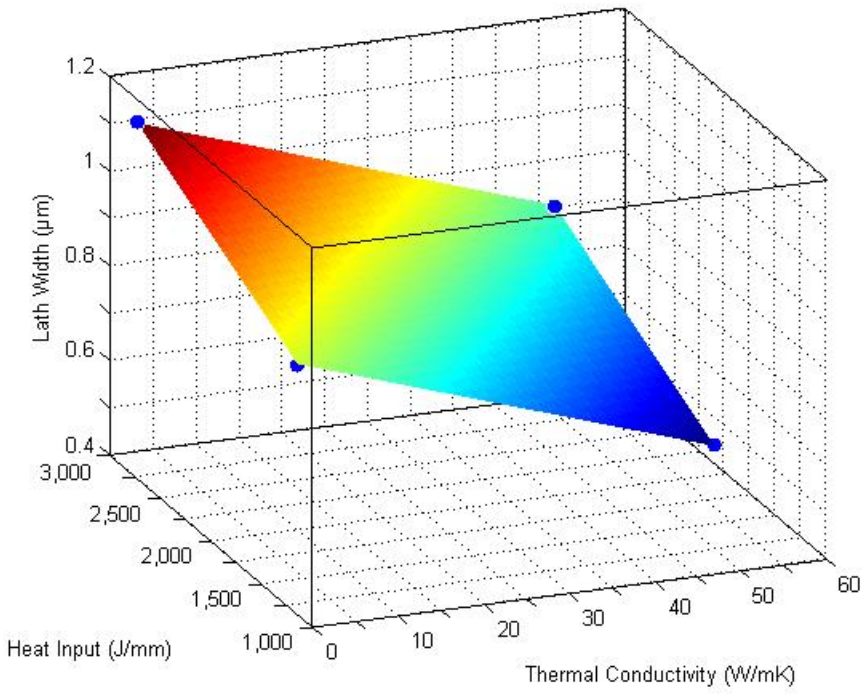

Figure 4-12 – Average lath width by thermal conductivity and heat input

Figure 4-12 shows that the lath width decreases with increased backing plate thermal conductivity and with decreased heat input. With a fixed backing plate, the lath width decreased by 0.22 µm as the heat input decreased by 1575 J/mm. Fixing the heat input decreased the lath width by 0.29 µm as the backing plate was changed from granite to steel.

Despite the changes in the lath width as the heat input and backing plate material vary, the lath width only differed by 0.07 µm (8%) for both 16 °C/s samples (Table 4-6 and Figure 4-10). The average lath width is plotted against the cooling rate in Figure 4-13.

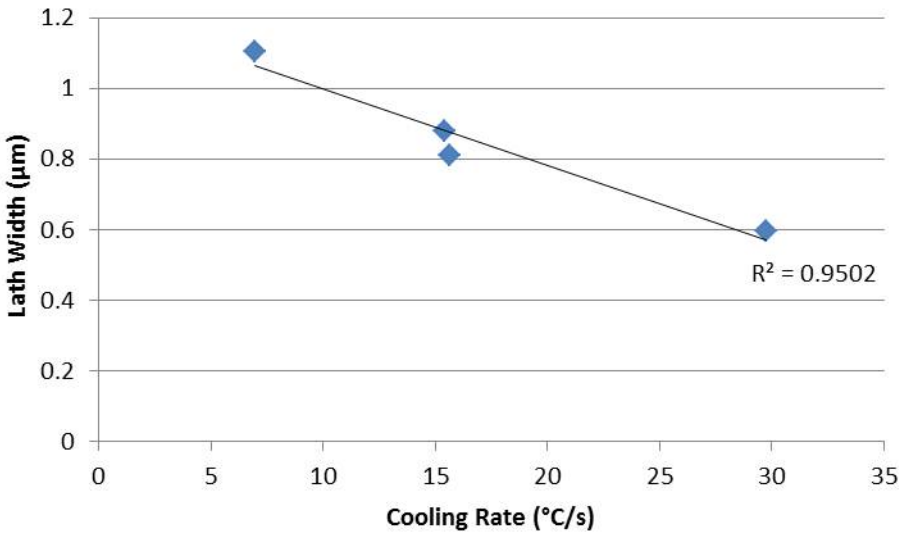

Figure 4-13 – Average lath width by cooling rate

There is a strong linear relationship between cooling rate and lath width, with lath width decreasing with increasing cooling rate. As the cooling rate is increased from 7 to 30 °C/s, the lath width is nearly halved from 1.11 to 0.59 µm.

This correlation between the cooling rate and the microstructure expands the findings of Wei. Wei observed that of the various rotational and travel speed relationships that have been developed for FSW, heat input had the best correlation to the microstructure [25]. The influence of heat input on cooling rate (Table 4-4 and Figure 4-2) points to the actual cause of this correlation being the changes that the process parameters have on the cooling rate.

Figure 4-14 compares the 95% hardness values to the lath width. There is a near perfect linear relationship between lath width and hardness. As the lath width decreased by 0.51 µm, the hard zone hardness increased by 27%, from 234 to 298 HV. This agrees with the Hall-Petch effect [33]. While the Hall-Petch effect measures grain size rather than lath size, most lath measurements also fit this linear hardness relationship [34].

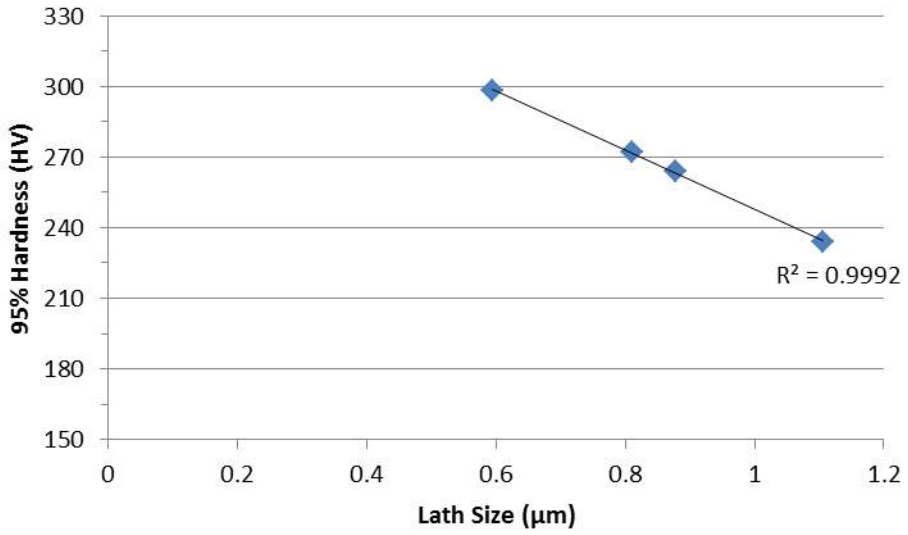

Figure 4-14 – Hard zone hardness by average lath width

Cooling rate is the driving factor behind the changes to the weld microstructure and mechanical properties in FSW. Each of the relationships in this study between cooling rate, hardness, and microstructure are strong linear relationships (Figure 4-8, Figure 4-13, and Figure 4-14). This confirms Allred and Matsushita's findings in physical weld simulations [21, 22] which point to cooling rate's effect on weld properties. Additionally, both the relationship between cooling rate and microstructure (CCT diagrams) and the relationship between the microstructure and the hardness (Hall-Petch effect) are based on fundamental principles of material science.

4.3 **Benefits of Cooling Rate Control**

Traditionally, cooling rate has been the result of changes to the travel speed on a fixed backing plate. This approach produced a range of 14 °C/s in this study (

Table 4-3). Combining the effects of both the backing plate and the heat input increased the range of possible cooling rates by 60%, to 23 °C/s. This allows for not only a 76% decrease

in the cooling rate, from 30 to 7 °C/s, but also an increase in the size of the process window for HSLA-65.

Previously reported process windows for HSLA-65 were limited by rotational and travel speeds [35]. These were expanded in this study through the use of backing plates of different thermal conductivity. Control over both heat input and backing plate enables the same desired cooling rate to be obtained over a range of parameters. This is demonstrated in the highlighted region of Figure 4-15.

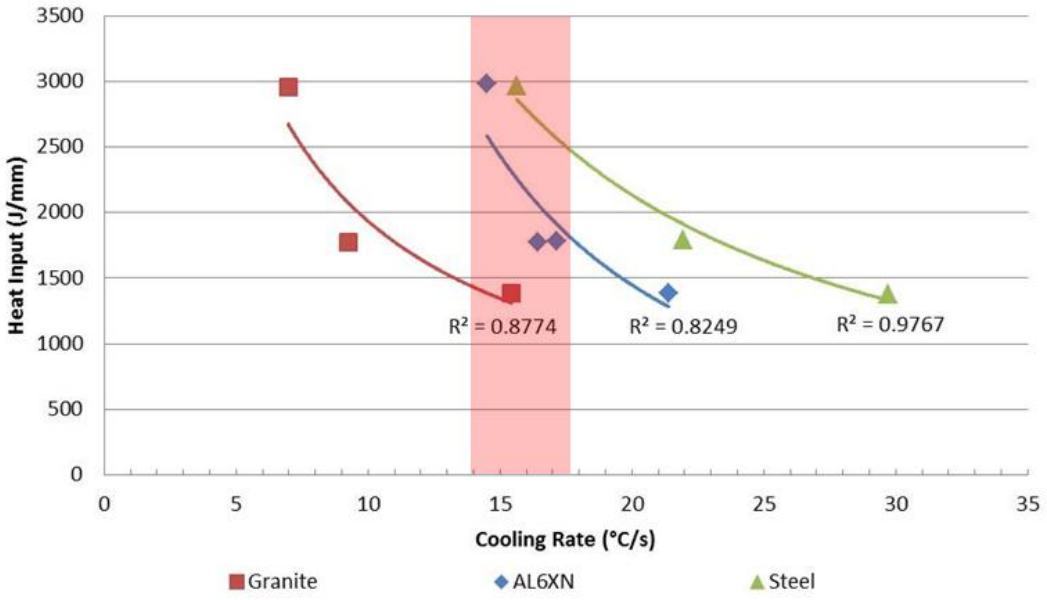

Figure 4-15 – Cooling rate vs heat input by backing plate material

Using only a steel backing plate (Figure 4-15), only one heat input can reach a cooling rate of 16 °C/s. By allowing for variation of the backing plate materials, this same cooling rate was achieved by five welds across the whole range of heat inputs. Obtaining 16 °C/s using the granite rather than the steel backing plate allowed for the travel speed to be tripled, from 76 to 229 mm/min (3 to 9 IPM, Table 3-2). Thus, the use of the backing plate as an additional process

parameter allows for greater weld productivity as well as the ability use cooling rate as a control variable.

If the statistical model for cooling rate (Table 4-4) extends beyond the limits of the experimental design of this study, then even lower cooling rates should be possible using backing plates of lower thermal conductivity or increasing the heat input. This would expand the process window even further and achieve even higher travel speeds.

5 CONCLUSIONS

The hard zone was previously believed to be the result of high peak temperatures or high heat inputs. In these welds, rotational and travel speed were used as the process parameters to affect both heat input and cooling rate. In this study, heat input and backing plate material were used as the process parameters to affect weld hardness. The following conclusions can be made:

- Cooling rate is the dominate factor affecting hard zone formation through its effects on weld microstructure. The lath width decreased linearly with increasing cooling rate, from 1.11 μm at 7 °C/s to 0.59 μm at 30 °C/s. This caused a strong linear increase in hard zone hardness, from 234 to 298 HV.
- The hard zone was eliminated by keeping the cooling rate below 20 °C/s and preventing the formation of bainite in HSLA-65.
- Decreasing the cooling rate increases the weld hardness uniformity and the weld microstructure homogeneity. The difference between the hard zone hardness and the average hardness decreased from a 14 to 5% difference as the cooling rate decreased from 30 to 7 °C/s.
- In addition to cooling rate, heat input also influences the lath size. With a fixed backing plate, the lath width increased by 0.22 μm as the heat input increased by 1575 J/mm. Across the same heat input increase, the length of the laths by at least 12 μm.

- Variation of the backing plate material allows for cooling rate to be used as a process parameter and expands the process window. The range of cooling rates was increased by 60%, from 14 °C/s on a steel backing plate, to 23 °C/s across all backing plates used in this study. Cooling rate control is demonstrated by five welds, across each heat input and backing plate level, being within 10% of 16 °C/s. Reaching 16 °C/s on a steel backing plate was only achieved using one heat input at 76 mm/min (3 IPM). Reaching the same cooling rate using a granite backing plate allowed for the travel speed to be tripled to 229 mm/min (9 IPM).

5.1 **Future Work**

The results of this study lead to several ideas for future investigations.

- Welding on backing plates of even lower thermal conductivity should be performed to try and increase travel speeds beyond what is current achievable in HSLA-65 steel.
- Further exploration is needed to understand the effect of different process parameters have on the cooling rate. Care should be taken to prevent the confounding of the heat input, power, and travel speed in further studies.
- Through improved temperature measurement in PCBN tools, temperature control can be accurately used in the FSW of steels. This will allow for an investigation into how temperature affects weld properties.

REFERENCES

[1] K. Sampath, "An understanding of HSLA-65 plate steels," *Journal of materials engineering and performance,* vol. 15, pp. 32-40, 2006.

[2] "ASTM A 945/A 945M - 06," in *Standard Specification for High-Strength Low-Alloy Structural Steel with Low Carbon and Restricted Sulfer for Improved Weldability, Formability and Toughness* vol. A 945/A 945M - 06. Conshohocken, PA: ASTM International, 2006.

[3] *High-Strength Structural and High-Strength Low-Alloy Steels*, 10th ed. vol. 1. Materials Park, OH: ASM International, 1990.

[4] P. R. Vishnu, *Solid-State Transformation in Weldments*, 10th ed. vol. 6. Materials Park, OH: ASM International, 1990.

[5] E. P. DeGarmo, *Materials and Processes in Manufacturing*, 9th ed. Hoboken, N.J.: Wiley, 2003.

[6] C. L. Tsai and C. M. Tso, *Heat Flow in Fusion Welding*, 10th ed. vol. 6. Materials Park, OH: ASM International, 1990.

[7] P. R. Vishnu, *Solid-State Transformations in Weldments*, 10th ed. vol. 6. Materials Park, OH: ASM International, 1990.

[8] S. Kou, *Welding Metallurgy*, 2nd ed. Hoboken, N.J.: Wiley-Interscience, 2003.

[9] J. F. Lancaster, *Metallurgy of Welding*: Chapman & Hall, 1993.

[10] F. P. Incropera, *Fundamentals of heat and mass transfer*: John Wiley, 2007.

[11] R. S. Mishra and M. W. Mahoney, Eds., *Friction stir welding and processing*. Materials Park, Ohio: ASM International, 2007, p. 360 p.

[12] W. Thomas*, et al.*, "Feasibility of friction stir welding steel," *Science and Technology of Welding & Joining,* vol. 4, pp. 365-372, 1999.

[13] A. Ozekcin*, et al.*, "A Microstructural Study of Friction Stir Welded Joints of Carbon Steels," *International Journal of Offshore and Polar Engineering,* vol. 14, 2004.

[14] R. Nandan*, et al.*, "Recent Advances in Friction-Stir Welding – Process, Weldment Structure and Properties," *Progress in Materials Science,* vol. 53, pp. 980-1023, 2008.

[15] P. J. Konkol and M. F. Mruczek, "Comparison of friction stir weldments and submerged arc weldments in HSLA-65 steel," *Welding Journal,* vol. 86, p. 187, 2007.

[16] S. C. Sanderson, "The Effect of Friction Stir Welding Process Parameters in Charpy V-Notch Impact Toughness in HSLA-65," Master of Science Master of Science, Department of Mechanical Engineering, Brigham Young University, Provo, UT, 2012.

[17] A. Tribe, "Study on the Fracture Toughness of Friction Stir Welded API X80 " Master of Science Master of Science, Department of Mechanical Engineering, Brigham Young University, Provo, UT, 2012.

[18] T. J. Lienert*, et al.*, "Friction Stir Welding Studies on Mild Steel," *Welding Journal,* pp. 1-9 S, 2003.

[19] T. W. Nelson*, et al.*, "Friction Stir Welding of X-65," *TMS,* vol. Friction Stir Welding and Processing IV, 2007.

[20] S. J. Anderson*, et al.*, "NSF-I/UCRC Center For Friction Stir Processing, Grant Number IIP-0437358," unpublished.

[21] M. Matsushita*, et al.*, "Microstructure and Toughness of Friction Stir Weld of 12 mm Thick Structural Steel," in *Twenty-first International Offshore and Polar Engineering Conference*, Maui, Hawaii, 2011, pp. 506-513.

[22] J. Allred, "Hard Zone Formation Mechanisms in Friction Stir Process X65," Brigham Young University, Provo, UT, 2013.

[23] W. Arbegast, "Modeling Friction Stir Joining as a Metalworking Process," *TMS,* vol. Hot Deformation of Aluminum Alloys III, p. 14, 2003.

[24] J. W. Pew, "A Torque-Based Weld Power Model for Friction Stir Welding," Master of Science, Department of Mechanical Engineering, Brigham Young University, Provo, UT, 2006.

[25] L. Wei, "Investigating Correlations of Microstructures, Mechanical Properties and FSW Process Variables in Friction Stir Welded High Strength Low Alloy 65 Steel," Doctor of Philosophy Doctor of Philosophy, Department of Mechanical Engineering, Brigham Young University, Provo, UT, 2009.

[26] D. W. Mayfield and C. D. Sorensen, "An Improved Temperature Control Algorithm for Friction Stir Processing," *International Friction Stir Welding Symposium,* vol. 8, 2010.

[27] K. A. Ross, "Investigation and Implementation of a Robust Temperature Control Algorithm for Friction Stir Welding," Master of Science Master of Science, Department of Mechanical Engineering, Brigham Young University, Provo, UT, 2012.

[28] P. Upadhyay and A. P. Reynolds, "Effects of Forge Axis Force and Backing Plate *Product Optimization Using Designed Experiments*: John Wiley & Sons, 2002.

[29] R. H. Myers and D. C. Montgomery, *Response Surface Methodology: Process and* Boundary Condition on FSW of AA6056," in *Friction Stir Welding and Processing VI*, R. S. Mishra*, et al.*, Eds.: TMS, 2011.

[30] H. K. D. H. Bhadeshia and R. W. K. Honeycombe, *Steels : Microstructure and Properties*, 3rd ed. Amsterdam ; Boston: Elsevier, Butterworth-Heinemann, 2006.

[31] "ANSI/API Spec 5L," in *Specification for Line Pipe* vol. API 5L Grade X65. Washington, DC: American Petroleum Institute 2007.

[32] S. Endo*, et al.*, "Advance in High Performance Linepipes with Respect to Strength and Deformability," presented at the International Conference on the Application and Evaluation of High-Grade Linepipes in Hostile Environments, Yokohama, Japan, 2002.

[33] W. D. Callister, *Materials science and engineering : an introduction*, 7th ed. New York: John Wiley & Sons, 2007.

[34] H. K. D. H. Bhadeshia, *Bainite in steels: transformations, microstructure and properties*: Institute of Materials, 1992.

[35] T. W. Nelson*, et al.*, "Friction stir welding of ferritic steels," in *Proceedings of ISOPE-2004: Fourteenth International Offshore and Polar Engineering Conference*, 2004.

APPENDIX A: STEEL TOOL DRAWING

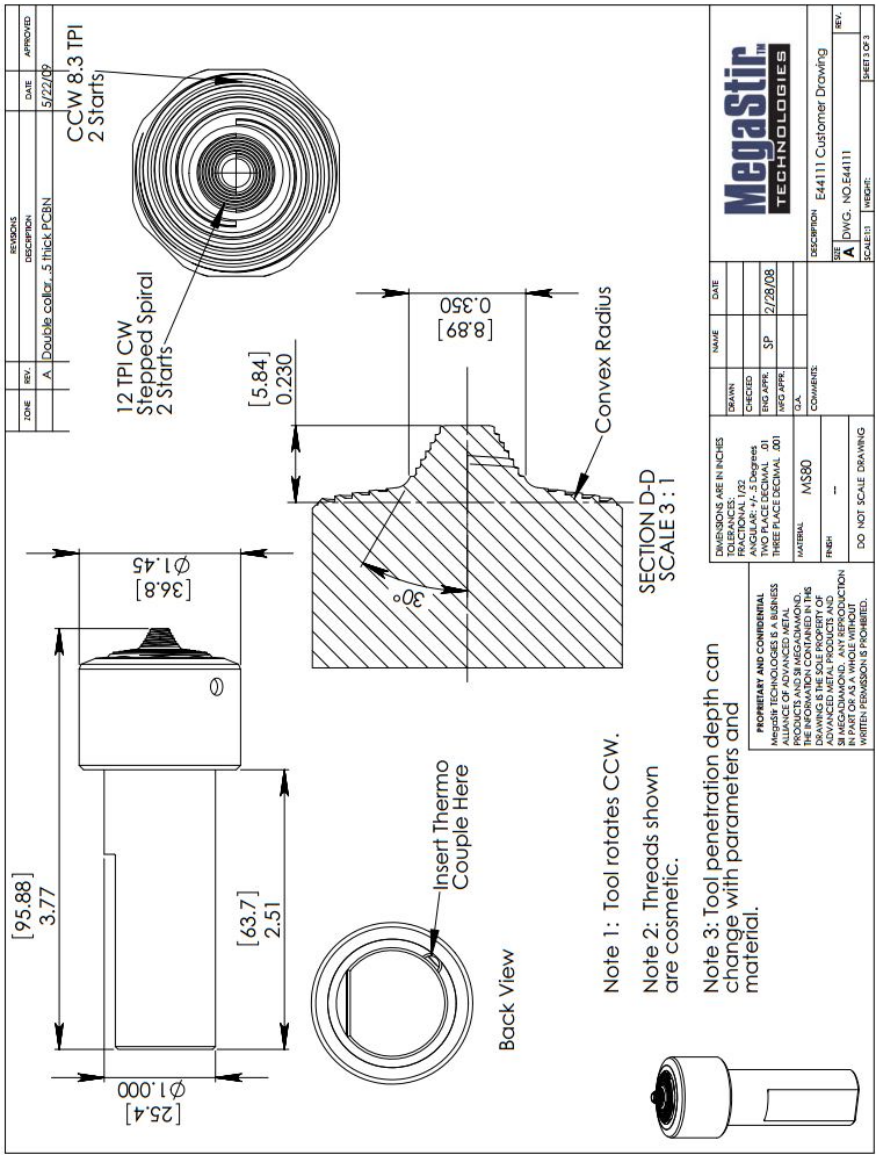

Figure A-1 – PCBN CS4 tool, model E44111

APPENDIX B: 95% HARDNESS

The use of the 95% hardness metric removes the need to choose an arbitrary hardness value to define the hard zone across all welds. The value is also independent of weld area. The selection of 95% rather than a higher percentage produces about 75 datapoints to characterize the high hardness area in each weld.

Table B- lists the various hardness characteristics and the corresponding cooling rate for each weld. Figure B-1, Figure B-2, and Figure B-3 plot the hardness values by rank for each weld on granite, AL6XN, and steel backing plates respectively.

Table B-1 – Hardness data and calculations for each weld

Weld ID	CR (°C/s)	Peak Hardness (HV)	95% Hardness (HV)	Average weld hardness (HV)	Increase (95%-Average,HV)	% Increase
GL	15.44	321	264	244.28	20	8.07%
GM	9.26	307	242	227.52	14	6.36%
GH	6.97	267	234	222.49	12	5.17%
AL	21.40	317	280	255.26	25	9.69%
AM1	17.14	292	264	240.93	23	9.58%
AM2	16.42	289	267	245.75	21	8.65%
AH	14.52	279	263	238.43	25	10.31%
SL	29.73	330	298	260.38	38	14.45%
SM	21.92	319	279	247.60	31	12.68%
SH	15.62	295	272	245.70	26	10.71%
Base	N/A	220	201	192.00	9	4.69%

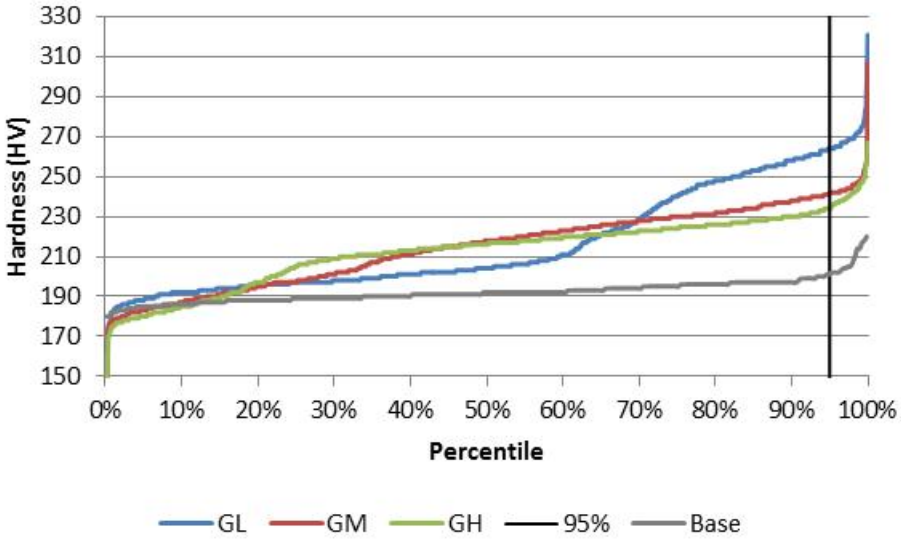

Figure B-1 – Percentile ranking charts for welds using a granite backing plate

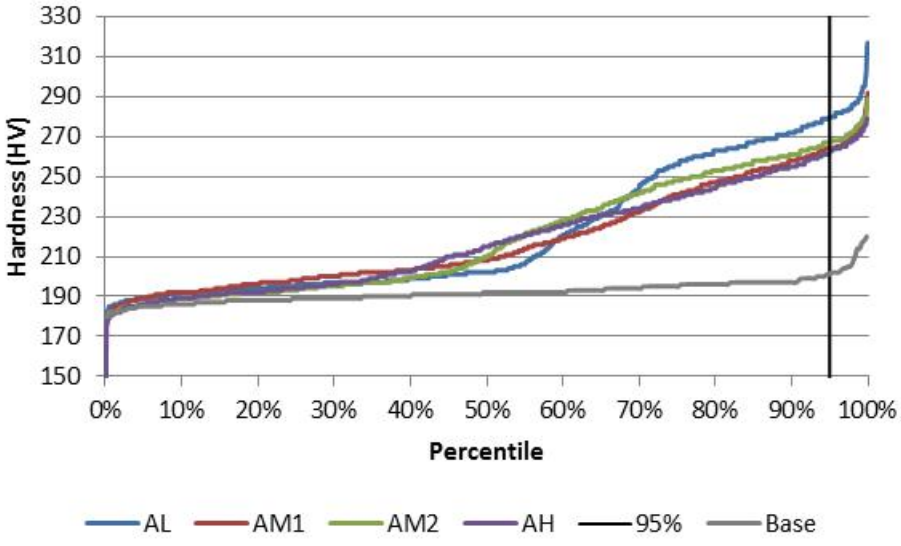

Figure B-2 – Percentile ranking charts for welds using an AL6XN backing plate

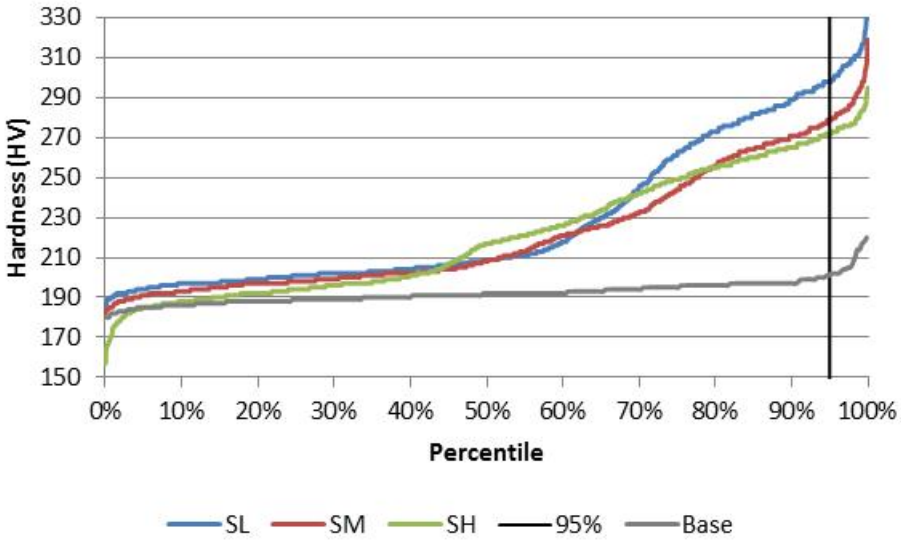

Figure B-3 – Percentile ranking charts for welds using a steel backing plate

APPENDIX C: WELD COOLING RATE AND TEMPERATURE DATA

Table C-1 – Full weld cooling rate and temperature data. Yellow boxes indicate a failure of the thermocouple and orange boxes represent averaged values

Run ID	Backing Plate Material	Heat Input (J/mm)		Cooling Rate - 0.18 in from weld center			Cooling Rate - 0.24 in from weld center			Cooling Rate - 0.30 in from weld center			Average Cooling Rates			Overall CR
		Desired	Calc.	a	b	c	a	b	c	a	b	c	0.18 in	0.24 in	0.30 in	Average
GL	Stone	1377.95	1386.18	15.51	14.49	15.01	15.24	14.33	14.96	17.12	15.29	16.96	15.00	14.85	16.46	15.44
GM	Stone	1771.65	1778.36	9.36	9.19	9.15		9.25	9.08		9.32	9.42	9.24	9.16	9.37	9.27
GH	Stone	2952.76	2953.28	6.70	6.71	7.22	6.81	6.75	7.10	6.82	6.86	7.71	6.88	6.88	7.13	6.97
AL	AL6XN	1377.95	1385.64	23.05	22.61	17.16	24.43	23.48	17.56	24.94	20.50	18.86	20.94	21.82	21.44	21.40
AM1	AL6XN	1771.65	1786.40	17.28	17.26	16.70	15.57	17.30	16.85	18.05	17.85	17.44	17.08	16.57	17.78	17.14
AM2	AL6XN	1771.65	1775.89	15.60	15.75	16.02	16.31	16.61	15.86	17.42	16.97	17.25	15.79	16.26	17.21	16.42
AH	AL6XN	2952.76	2977.96	14.02	14.48	14.15		14.82	14.43	14.49	14.72	14.95	14.22	14.63	14.72	14.60
SL	Steel	1377.95	1379.82	30.51	28.59	26.58	31.40	30.60	28.32	31.77	30.29	29.48	28.56	30.11	30.51	29.73
SM	Steel	1771.65	1787.38	21.02	20.46	20.57		21.61	21.68	24.78	23.42	22.09	20.69	21.65	23.43	21.47
SH	Steel	2952.76	2962.10	16.38	14.16	11.40	15.97	14.16	11.69	18.94			13.98	13.94	18.94	13.96

Run ID	Backing Plate Material	Heat Input (J/mm)		Peak Temperature - 0.18 in from weld center			Peak Temperature - 0.24 in from weld center			Peak Temperature - 0.30 in from weld center			Average Peak Temperatures			Peak Tool Temp
		Desired	Calc.	a	b	c	a	b	c	a	b	c	0.18 in	0.24 in	0.30 in	
GL	Stone	1377.95	1386.18	1038.47	1057.87	1104.26	964.31	1013.06	982.77	872.37	916.91	918.01	1066.87	986.71	902.43	916.16
GM	Stone	1771.65	1778.36	1190.28	1188.49	1203.62		1137.94	1133.87		1042.13	1059.85	1194.13	1135.91	1050.99	971.87
GH	Stone	2952.76	2953.28	1327.38	1238.06	1238.97	1223.38	1188.42	1214.78	1174.21	1158.76	1109.21	1268.14	1208.86	1147.39	987.29
AL	AL6XN	1377.95	1385.64	1026.38	1041.75	1167.84	948.63	955.86	1011.08	855.62	892.75	953.36	1078.66	971.86	900.58	919.86
AM1	AL6XN	1771.65	1786.40	946.47	949.16	973.24	932.12	955.21	953.50	896.74	916.81	920.86	956.29	946.94	911.47	928.28
AM2	AL6XN	1771.65	1775.89	998.24	984.61	994.37	930.68	955.21	915.36	873.31	870.06	854.62	992.41	933.75	866.00	952.80
AH	AL6XN	2952.76	2977.96	1066.08	1015.14	1089.81		995.82	990.91	988.11	983.86	990.90	1057.01	993.37	987.62	949.55
SL	Steel	1377.95	1379.82	1019.04	1102.46	996.45	878.43	868.21	866.14	818.08	827.57	827.08	1039.32	870.93	824.24	904.25
SM	Steel	1771.65	1787.38	910.69	940.74	931.01		901.29	903.34	852.45	834.20	831.10	927.48	902.32	839.25	932.14
SH	Steel	2952.76	2962.10	1010.39	1029.36	1030.68	991.19	984.48	991.70	935.97	914.26		1023.48	989.12	925.11	962.60

APPENDIX D: HARDNESS MAPS

HSLA 65, BP - Granite, 2953 J/mm, GH

Vickers Micro-Hardness

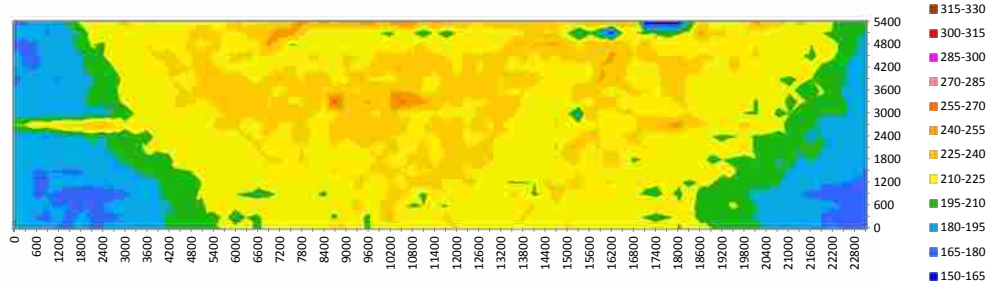

HSLA 65, BP - Granite, 1772 J/mm, GM

Vickers Micro-Hardness

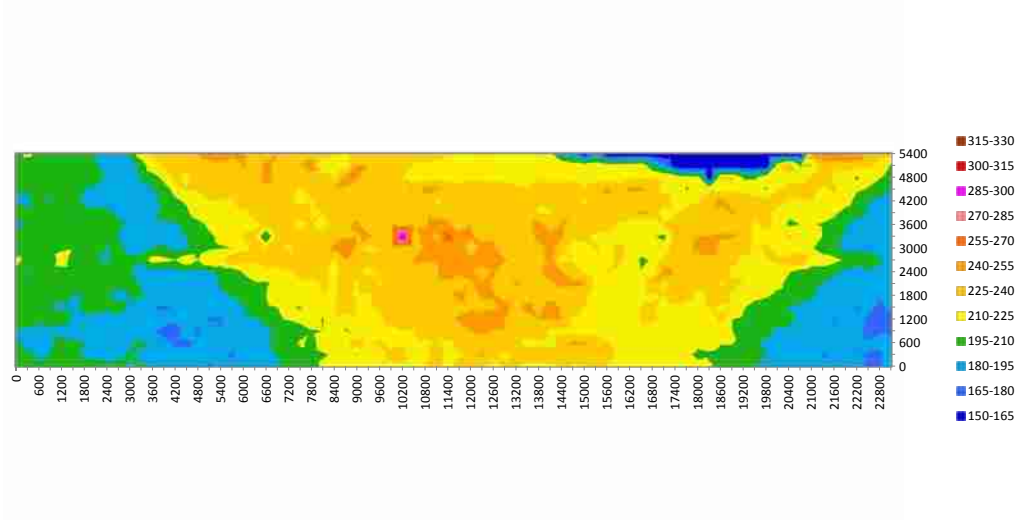

HSLA 65, BP - Granite, 1378 J/mm, GL

Vickers Micro-Hardness

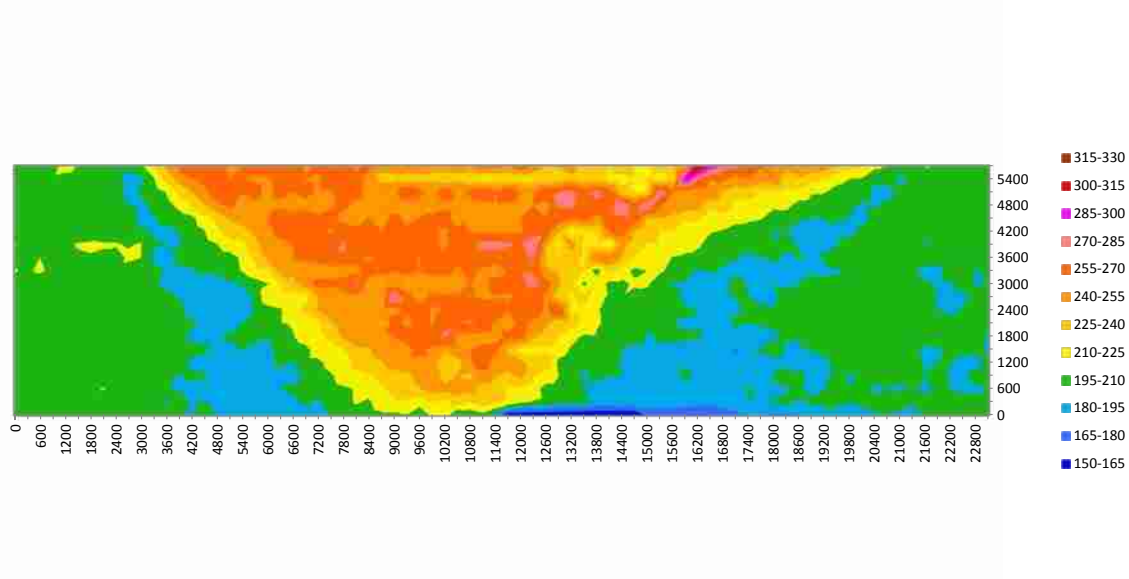

HSLA 65, BP - AL6XN, 2953 J/mm, AH

Vickers Micro-Hardness

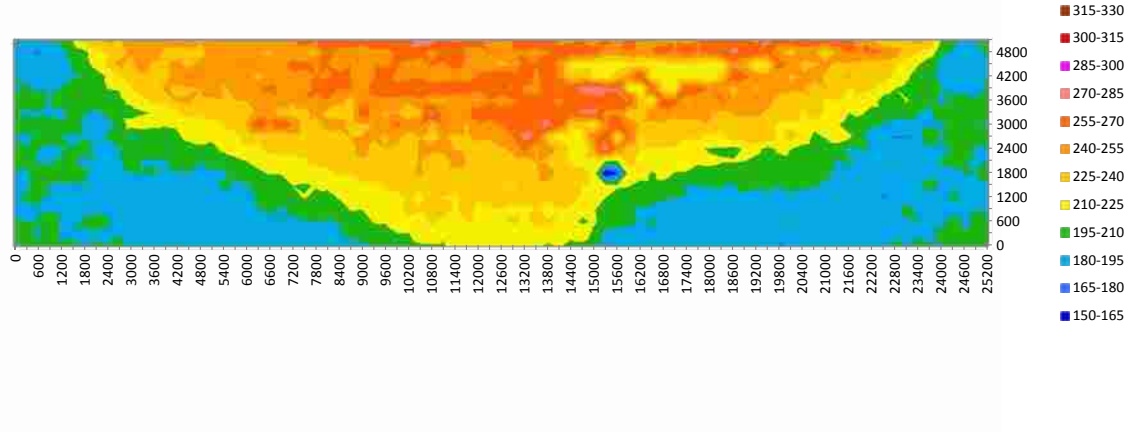

HSLA 65, BP - AL6XN,1772 J/mm, AM1

Vickers Micro-Hardness

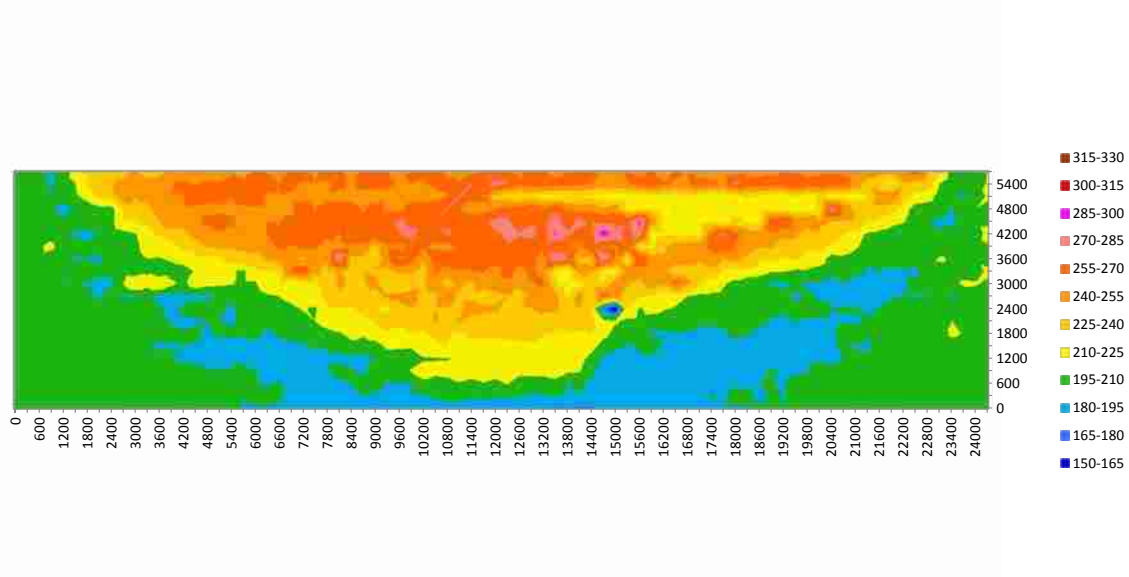

HSLA 65, BP - AL6XN,1772 J/mm, AM2

Vickers Micro-Hardness

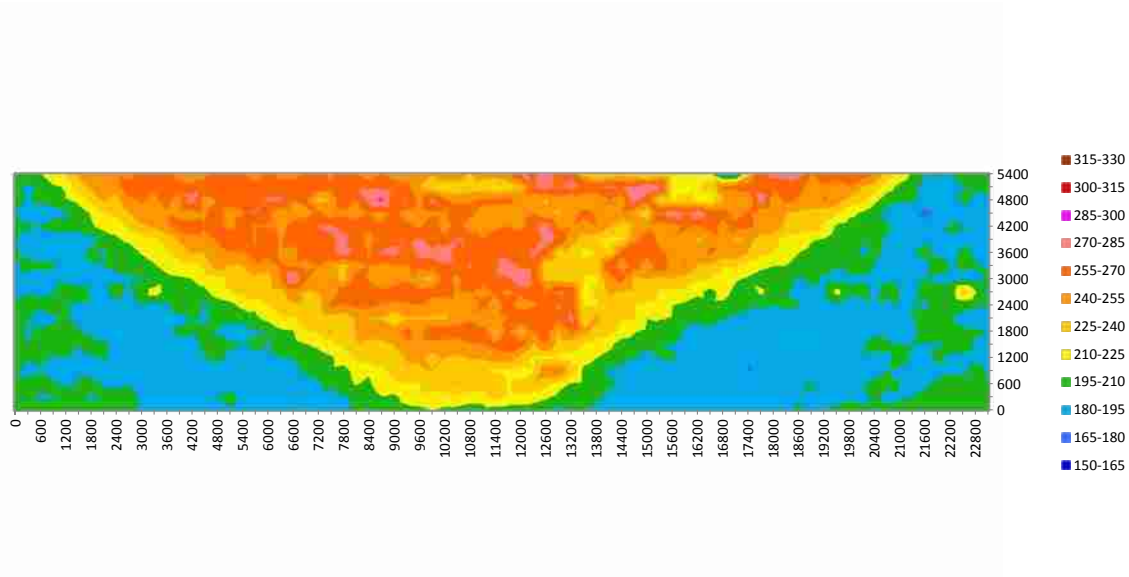

HSLA 65, BP - AL6XN, 1378 J/mm, AL

Vickers Micro-Hardness

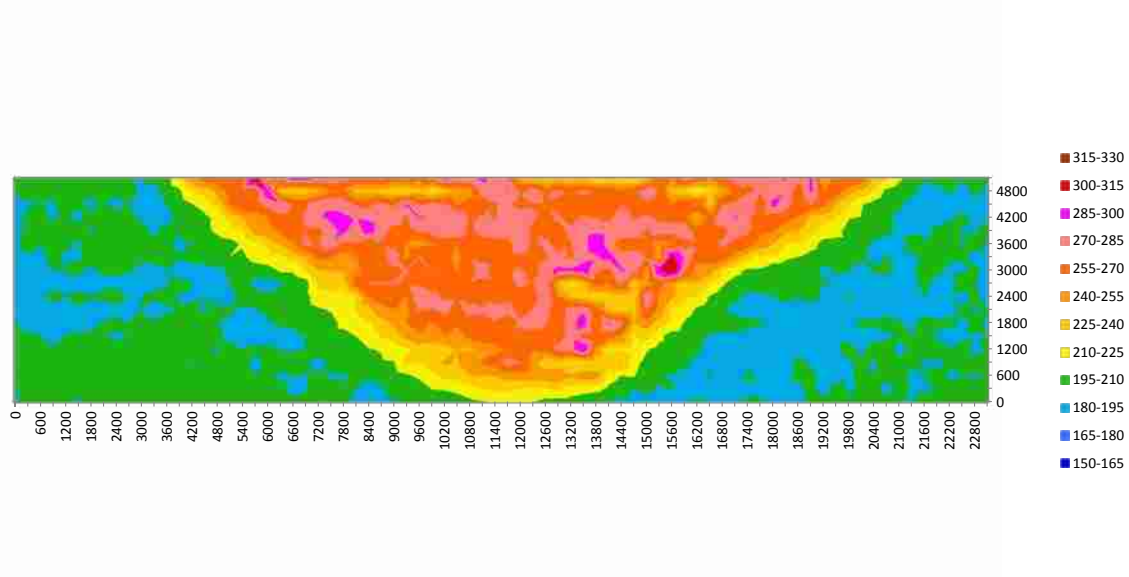

HSLA 65, BP - Steel, 2953 J/mm, SH

Vickers Micro-Hardness

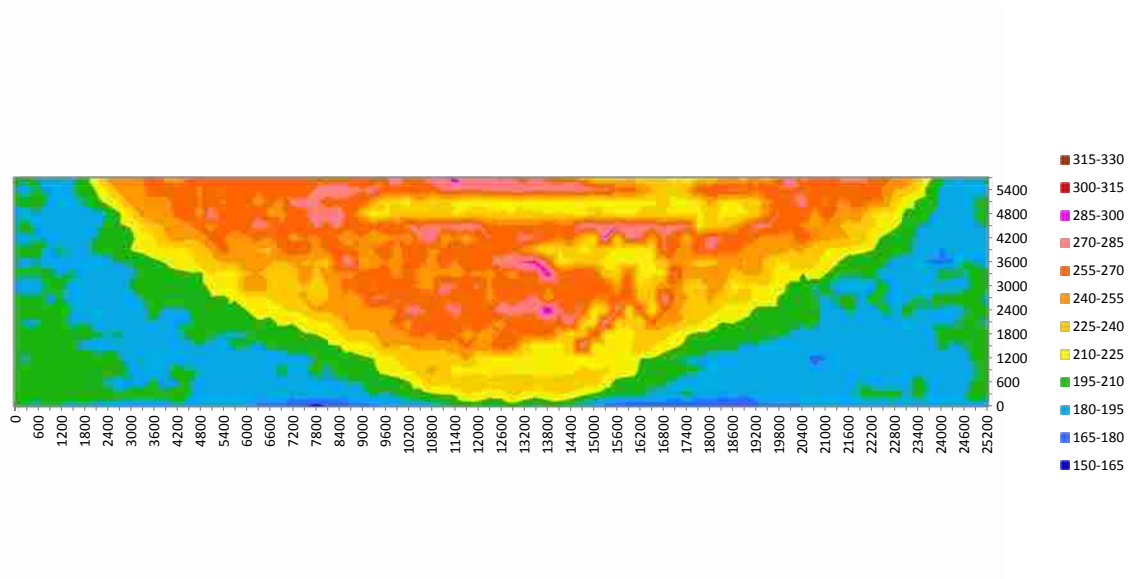

HSLA 65, BP - Steel, 1772 J/mm, SM

Vickers Micro-Hardness

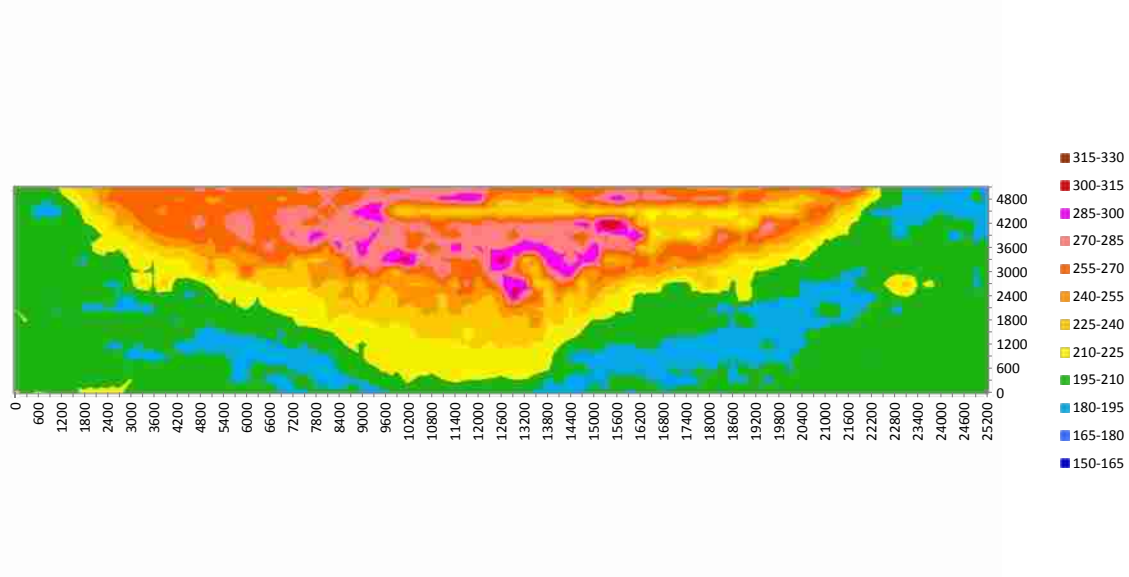

HSLA 65, BP - Steel, 1378 J/mm, SL

Vickers Micro-Hardness

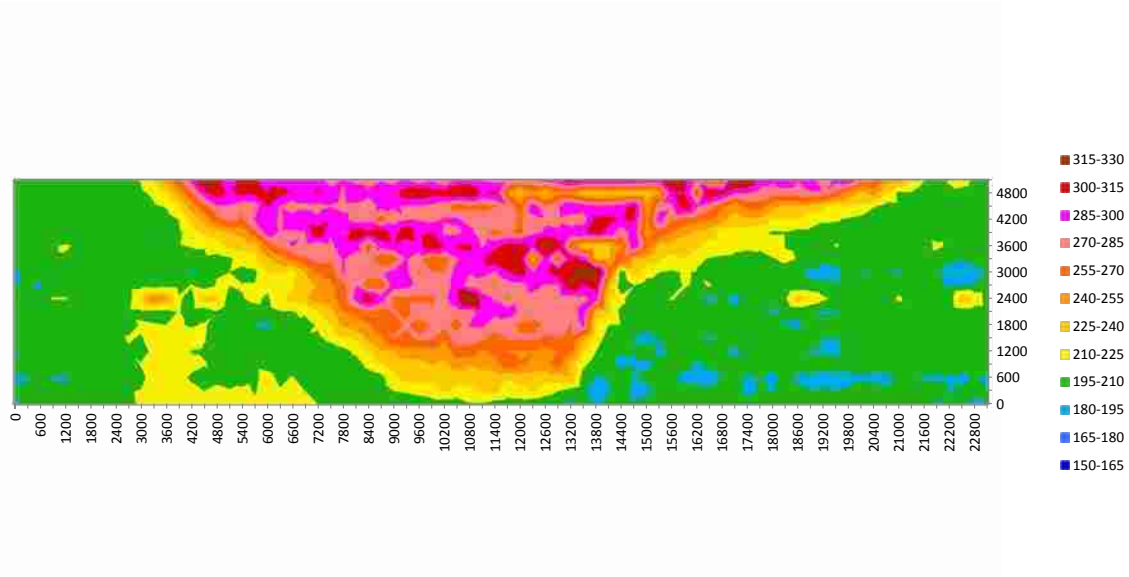

APPENDIX E: LATH LENGTH MEASUREMENTS

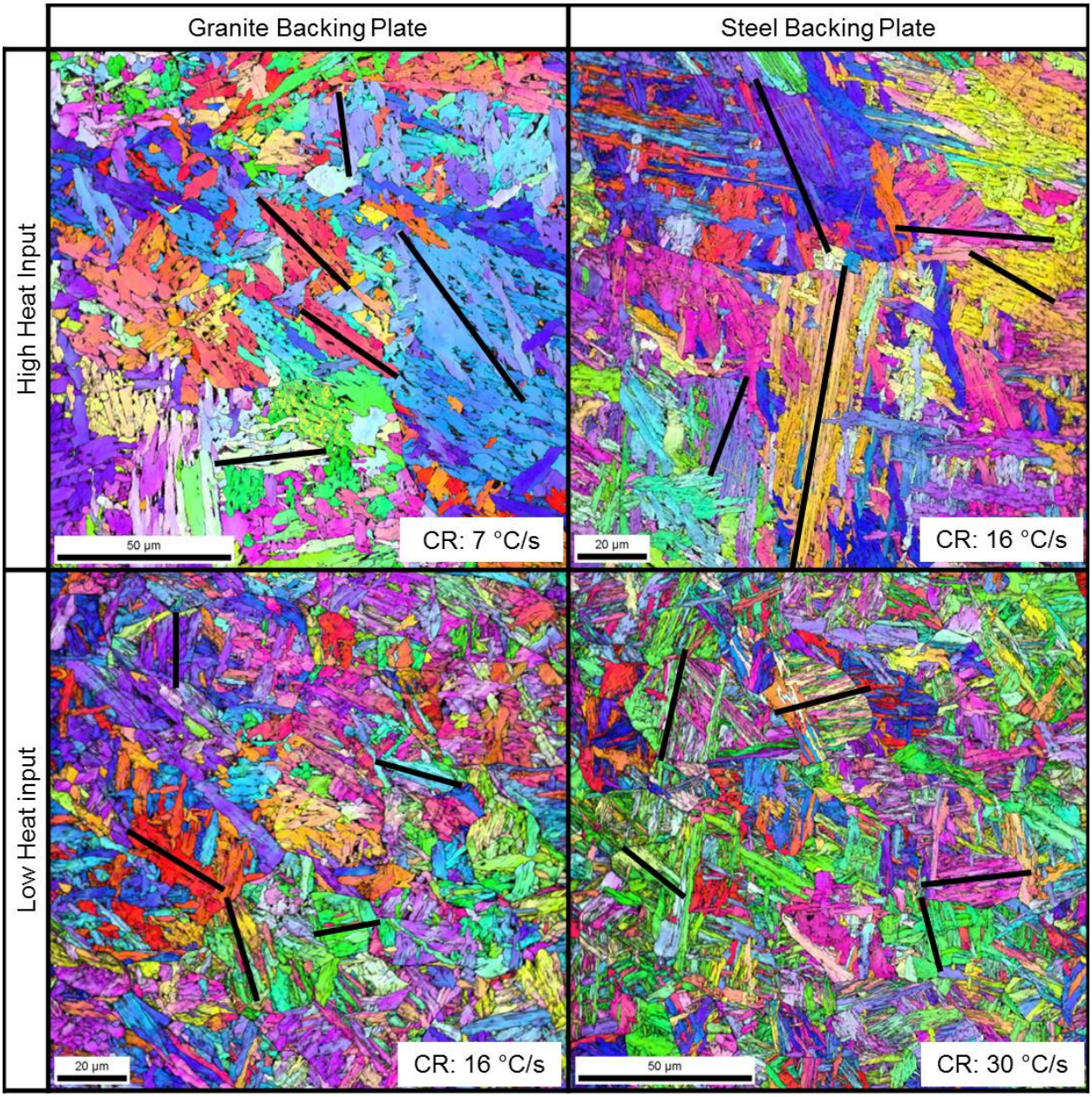

Figure E-1 – Locations of lath length measurements

Table E-1 – Lath measurements for each packet measured

Sample	Lath Lengths (µm)					
	Packet 1	Packet 2	Packet 3	Packet 4	Packet 5	Average
GH	34.17	50.49	35.49	27.56	24.59	34.46
GL	12.74	22.72	20.86	16.37	27.52	20.04
SH	18.73	34.67	62.37	28.52	33.15	35.49
SL	16.26	27.39	25.14	18.81	23.83	22.29